Title: Fetal programming by the maternal microbiome of offspring behavior, and DNA methylation and gene expression within the hippocampus

Authors:

Kevin L. Gustafson[1,2], Susheel Bhanu Busi[3,4], Zachary L. McAdams[1], Rachael E. McCorkle[2], Pavlo Khodakivskyi[5], Nathan J. Bivens[6], Daniel J. Davis[1,7], Murugesan Raju[8], Lyndon M. Coghill[1,8], Elena A. Goun[5], James Amos-Landgraf[1,2,9,10], Craig L. Franklin[1,2,9,10], Paul Wilmes[11], Rene Cortese[12], and Aaron C. Ericsson[1,2,9,10]

Affiliations:

[1]Department of Veterinary Pathobiology, College of Veterinary Medicine, University of Missouri, Columbia, MO, USA

[2]College of Veterinary Medicine, University of Missouri, Columbia, MO, USA

[3]Luxembourg Centre for Systems Biomedicine, University of Luxembourg, Esch-sur-Alzette, Luxembourg

[4]UK Centre for Ecology and Hydrology, Wallingford, Oxfordshire, UK

[5]Department of Chemistry, College of Arts and Science, University of Missouri, Columbia, MO, USA

[6]University of Missouri Genomics Technology Core, University of Missouri, Columbia, MO, USA

[7]University of Missouri Animal Modeling Core, University of Missouri, Columbia, MO, USA

[8]University of Missouri Bioinformatics and Analytics Core, University of Missouri, Columbia, MO, USA

[9]University of Missouri Mutant Mouse Resource and Research Center (MMRRC)

[10]University of Missouri Metagenomics Center, University of Missouri, Columbia, MO, USA

[11]Department of Life Sciences and Medicine, Faculty of Science, Technology and Medicine, University of Luxembourg, Esch-sur-Alzette, Luxembourg

[12]Department of Child Health & Obstetrics, Gynecology, and Women's Health, School of Medicine, University of Missouri, Columbia, MO, USA

Corresponding author: ACE at ericssona@missouri.edu

The microorganisms colonizing the gastrointestinal tract of animals, collectively referred to as the gut microbiome, affect numerous host behaviors dependent on the central nervous system (CNS). Studies comparing germ-free mice to normally colonized mice have demonstrated influences of the microbiome on anxiety-related behaviors, voluntary activity, and gene expression in the CNS. Additionally, there is epidemiologic evidence supporting an intergenerational influence of the maternal microbiome on neurodevelopment of offspring and behavior later in life. There is limited experimental evidence however directly linking the maternal microbiome to long-term neurodevelopmental outcomes, or knowledge regarding mechanisms responsible for such effects. Here we show that that the maternal microbiome has a dominant influence on several offspring phenotypes including anxiety-related behavior, voluntary activity, and body weight. Adverse outcomes in offspring were associated with features of the maternal microbiome including bile salt hydrolase gene expression (*bsh*), abundance of certain bile acids, and hepatic expression of *S1pr2*. In cross-foster experiments, offspring resembled their birth dam phenotypically, despite faithful colonization in the postnatal period with the surrogate dam microbiome. Genome-wide methylation analysis of hippocampal DNA identified microbiome-associated differences in methylation of 196 loci in total, 176 of which show conserved profiles between mother and offspring. Further, single-cell transcriptional analysis revealed accompanying differences in expression of several differentially methylated genes within certain hippocampal cell clusters, and vascular expression of genes associated with bile acid transport. Inferred cell-to-cell communication in the hippocampus based on coordinated ligand-receptor expression revealed differences in expression of neuropeptides associated with satiety. Collectively, these data provide proof-of-principle that the maternal gut microbiome has a dominant influence on the neurodevelopment underlying certain offspring behaviors and activities, and selectively affects genome methylation and gene expression in the offspring CNS in conjunction with that neurodevelopment.

Main

Anxiety disorders (AD) are increasing in prevalence, affecting close to 1 in 10 children and adolescents between the ages of 3 and 17[1]. Like most mood disorders, AD are multifactorial and often result from a combination of genetic, environmental, and experiential factors. Similarly, one in five children in the U.S. are obese or overweight[2], reflecting the combined influence of western diet, increasingly sedentary lifestyles, and other factors. Moreover, AD and obesity/overweight (OO) are reciprocal risk factors, frequently occurring as co-morbidities[3-7]. A growing body of research has linked the gut microbiome

59 (GM) to neurodevelopment and behavior[8-13], and growth rate or weight gain[14-17]. Work with germ-free
60 mice shows the importance of the GM in normative behavior and metabolism[18-20], and transfer of an
61 anxiety-related phenotype or increased energy harvest via fecal microbiome transfer indicates that
62 certain features within naturally occurring microbiomes influence these phenotypes[21-23]. There are also
63 developmental components to both AD and OO, raising the question of how the maternal microbiome
64 during pregnancy affects fetal development and subsequent behavior and energy metabolism in the
65 adult offspring. The maternal gut microbiome during pregnancy produces metabolites which reach
66 peripheral circulation and the fetal CNS[24], and maternal proteins and peptides produced by
67 enteroendocrine cells in response to the microbiome likely also cross the placenta and reach fetal
68 circulation[25-27]. Disruption of the maternal GM can affect these processes as demonstrated by increased
69 anxiety in the offspring of mice with antibiotic- or diet-induced dysbiosis[28-31].
70 There are still major gaps in our knowledge however regarding the mechanisms through which the
71 maternal microbiome during pregnancy programs long-lasting changes in offspring behavior and
72 metabolism. These intergenerational effects suggest fetal programming by an unknown mechanism,
73 while differences in anxiety-related behavior (and other complex behaviors) indicate a
74 neurodevelopmental basis. Owing to the genetic, dietary, and environmental heterogeneity, analysis of
75 these processes in a human population requires impossibly large sample sizes and long-term tracking of
76 mother-child pairs. Here, we use two groups of genotype-, age-, and sex-matched outbred mice,
77 colonized with one of two naturally occurring microbiomes associated with differences in anxiety-
78 related behavior, voluntary activity, fetal growth, food intake, and adult growth. Cross-foster studies
79 demonstrate the dominant influence of the maternal microbiome on offspring phenotypes. Further
80 analysis of hippocampal DNA revealed selective effects of the maternal microbiome on CpG
81 methylation, maintained in offspring independent of the postnatal microbiome. Single-nuclei RNA
82 sequencing (snRNA-seq) of hippocampal RNA confirmed fetal programming of several cell-specific
83 differentially methylated genes, including genes involved in pathways that are orexigenic in nature and
84 important for cell-to-cell contact.
85
86 **Complex microbiome-dependent behaviors determined by maternal microbiome**
87 To identify the developmental period in which the microbiome exerts its effects, we used an
88 experimental design with four groups, comprising mice born to dams harboring GM^{Low} (originating from
89 the Jackson Laboratory, Bar Harbor, ME) or GM^{High} (originating from Envigo, Madison, WI) and remaining
90 with their birth dams until weaning (control), or cross-fostered at birth to nursing dams harboring the

91 reciprocal microbiome (**Fig. 1a**). These groups are denoted as CF^{Low} and CF^{High}, with the microbiome
92 designation indicating the postnatal offspring composition acquired via cross-foster (CF). Comparisons
93 were then made between the two control groups, and between the two CF groups, in behavior tests
94 associated with anxiety-related behavior and voluntary activity between five and seven weeks of age,
95 and body weight (BW) at three and seven weeks of age.
96 In agreement with previous studies, age-, sex-, and genotype-matched mice colonized with GM^{Low} spent
97 less time and traveled less distance in the light portion of a light-dark transition (LDT) test (**Fig. 1b,**
98 **Extended Data Fig. 1a**), and the open arms of an elevated plus maze (EPM) test (**Fig. 1c, Extended Data**
99 **Fig. 1b**), relative to mice colonized with GM^{High}, indicating differential effects on anxiety-related behavior
100 of the two microbiomes. No behavioral differences were observed in the open-field exploration test
101 between GM^{Low} and GM^{High} mice (**Extended Data Fig. 1c-d**). To assess voluntary activity, mice were singly
102 housed with bluetooth wireless running wheels for a five-day acclimation period followed by seven-day
103 test period. Both male (**Fig. 1d**) and female (**Fig. 1e**) mice colonized with GM^{High} ran significantly more
104 than mice with GM^{Low} ($p < 0.0001$, F = 29.2, and $p = 0.0002$, F = 14.4, respectively). Previously reported
105 differences in body weight (BW) at weaning (**Extended Data Fig 1e**) and adulthood (**Fig. 1f**, $p < 0.0001$, F
106 = 24.7) were also reproducible. Collectively, these data confirmed microbiome-associated differences in
107 anxiety-related behavior, voluntary activity, and body weight, in sex-, age-, and genotype-matched
108 mice.
109 The GM-associated differences in the LDT, independent of sex, were reversed in the comparison
110 between CF^{Low} and CF^{High} mice, with the latter demonstrating behavior suggestive of greater anxiety (**Fig.**
111 **1g, Extended Data Fig. 1f**). Similarly, the robust GM-dependent differences in the EPM were abrogated
112 in the CF^{Low} and CF^{High} mice (**Fig. 1h, Extended Data Fig. 1g**) indicating that the maternal microbiome has a
113 substantial, if not dominant, influence on neurodevelopmental events contributing to anxiety-related
114 behavior in the offspring. While a significant difference of total distance traveled in the OFE test was
115 observed, distance traveled in the center was not found to be significant in the cross-foster groups
116 **(Extended Data Fig 1. h-i)**. The significant GM-associated differences in voluntary activity were absent in
117 male and female CF mice (**Fig. 1i-j**). Comparison of BW revealed no difference at weaning (**Extended**
118 **Data Fig. 1j**) and reversal in adulthood (**Fig. 1k**), such that CF^{High} mice weighed more than age-matched
119 CF^{Low} mice. These findings suggest that the neurodevelopmental processes contributing to the
120 microbiome-associated difference in BW and voluntary activity are also subject to some degree of
121 influence on fetal development, presumably via the maternal microbiome. Moreover, they raise the
122 possibility of a connection between the anxiety-related behaviors and the behaviors underlying the

123 difference in BW and voluntary activity, representing a constellation of behavioral phenotypes
124 influenced by features within the microbiome. Bacterial 16S rRNA amplicon sequencing was used to
125 confirm that CF mice harbored a microbiome of comparable richness and beta-diversity to that present
126 in surrogate dams, in both directions of transfer (**Extended Data Fig. 2a-c**).
127
128 **Taxonomic differences are associated with different levels of biologically relevant metabolites**
129 Compositional differences between GM^{Low} and GM^{High} have been described previously[32-34], including
130 greater richness in GM^{High} compared to GM^{Low} (**Fig. 2a**). Families enriched in GM^{Low} included
131 *Erysipelatoclostridiaceae*, *Erysipelotrichaceae*, *Sutterellaceae*, *Saccharimonadaceae*, *Acholeplasma-*
132 *taceae*, and unresolved members of orders *Tissierellales* and RF39; while families enriched in GM^{High}
133 included *Prevotellaceae*, *Marinifilaceae*, *Clostridiaceae*, *Desulfovibrionaceae*, *Deferribacteraceae*, and an
134 unresolved family within the order *Rhodospirillales* (**Supplementary Table 1**). We next asked the
135 question of whether differences in the GMs are also associated with distinct metabolite profiles. To this
136 end, fecal samples were collected from both male and female GM^{Low} and GM^{High} mice, and a
137 combination of mass spectrometry (MS)-based platforms were used to measure short-chain fatty acids;
138 branched chain fatty acids, branched chain keto-acids, and other lipids; unconjugated primary and
139 secondary bile acids (BAs); all proteinogenic amino acids and several nonproteinogenic and acetylated
140 amino acids; tryptophan derivatives including kynurenine, serotonin, and several indoles; B vitamins;
141 dicarboxylic acids; glucose, fructose, and other compounds in glycolysis; all ribonucleosides and
142 nitrogenous bases; compounds within the pentose phosphate pathway; compounds within the classic
143 TCA cycle; and other biologically relevant microbial metabolites (Full list of metabolites **Supplementary**
144 **Table 2, Supplementary Table 3**). GM^{Low} and GM^{High} showed differences in sugar molecules involved in
145 metabolism, multiple amino acids, and bile acids (**Fig. 2b**) (**Supplementary Table 2**). Interestingly, BAs
146 were among the metabolites enriched in the feces of mice harboring GM^{High}. These patterns were
147 apparent in the feces of male mice (**Extended Data Fig. 3a**), while female mice showed a single BA
148 (lithocholic acid) enriched in the feces of GM^{Low} (**Extended Data Fig. 3b**). We next asked whether
149 differences in the fecal metabolites would translate to differences in metabolites entering vascular
150 circulation. Serum, concurrently collected at the time of fecal collection, was subjected to MS.
151 Remarkably, the only significant difference in the metabolite profiles of the serum, was a BA (**Fig.**
152 **2c**)(**Supplemental Table 3**). There were also several BAs, both primary and secondary, that did not reach
153 statistical significance but had high levels within the serum of individual GM^{Low} mice. This pattern was
154 evident in the serum of female, but not male mice (**Extended Data Fig. 3c-d**). To examine whether this

155 difference in bile acids may have a physiological affect, we performed quantitative RT-PCR with mRNA
156 from both ileal and hepatic tissue for genes known to be involved in BA cellular transport. *Asbt*, a gene
157 involved in transporting BAs from the ileal lumen into the ileal epithelium showed no difference in
158 expression (**Fig. 2d**). Expression of *Ost-β*, a gene involved in transport of BAs from the ileal epithelium
159 into peripheral circulation, was increased in GM^{High} mice (**Fig. 2e**). *Gpbar1*, a G protein-coupled BA
160 receptor, was found to have increased expression in the ileum of GM^{Low} mice (**Fig. 2f**). In contrast, the
161 nuclear BA receptor *Fxr*, involved in regulation of bile acid production, showed no difference in ileal
162 expression (**Fig. 2g**). Accordingly, *Cyp7a1*, a gene downstream of *Fxr* that encodes the rate-limiting step
163 in bile acid synthesis, showed no difference in hepatic expression (**Fig. 2h**). Of note, expression of the
164 vascular BA transporter *Slc10a1* was increased in the liver of GM^{Low} mice (**Fig. 2i**) as was *S1pr2*, a non-
165 canonical G protein-coupled BA receptor (**Fig 2j**).
166 We examined whether bile salt hydrolase (BSH), the enzyme bacteria use to deconjugate bile acids, was
167 transcriptionally of functionally different between the GMs of female mice. While total gene read count
168 did not differ (**Extended Data Fig. 3e**), expression of *bsh* was significantly higher in GM^{Low} (**Extended**
169 **Data Fig. 3f)**. The BSH family of enzymes is widely expressed among gut bacteria, and prone to
170 significant variations in structure with some isoforms exhibiting different deconjugation activity toward
171 various bile acids and possessing various levels of enzymatic activities[35, 36]. Thus, we compared BSH
172 enzymatic activities of both microbiomes toward various bile acids. Our results demonstrated
173 significantly greater BSH activity specific for cholic acid in GM^{Low}, but no other differences were detected
174 in BSH activities towards other BAs examined (**Extended Data Fig. 3g-k**). Collectively, these data indicate
175 that there are numerous differentially abundant GM associated serum metabolites including several BA
176 species accompanied by differences in ileal and hepatic expression of genes encoding bile acid
177 transporters and receptors.
178
179 **Fetal programming of gene methylation in hippocampus by the maternal microbiome**
180 Reasoning that an influence on offspring behavior by the maternal microbiome must have a biological
181 foundation in the CNS and a mechanism by which cellular function and gene expression are established
182 during fetal development, we next examined gene expression and its epigenetic regulation in offspring
183 hippocampus, given its central role in anxiety-related behavior[37-42]. To identify effects of the maternal
184 microbiome on fetal programming of DNA methylation in the hippocampus, we performed genome-
185 wide DNA methylation profiling in female mice.

186 Analysis of methylation across the entire array, and parallel comparisons between samples from GM^{Low}
187 or GM^{High} mice, and from CF^{Low} or CF^{High} mice, identified only 196 differentially methylated markers
188 (DMRs) with beta values differing by $\log_2 FC > 1$ (**Supplementary Table 4**). Remarkably, 176 of those 196
189 sites (89.8%) showed a difference in methylation at the same site in the reciprocal contrast, such that
190 offspring methylation matched that of their birth dam (**Fig. 3a, $R^2 = -0.644$, $p = 2 \times 10^{-7}$**). DMRs identified
191 in offspring hippocampi were distributed across the genome, occurring most often early in gene bodies
192 or enhancer/promoter regions and roughly correlating in frequency to chromosomal gene content, with
193 the exception of an apparent enrichment for DMRs on chromosome 14 (**Fig. 3b, $p = 0.003$**). Differential
194 methylation was detected at five contiguous markers mapped to promoters, enhancers, and exon 1 of
195 the *Pde1c* gene, encoding phosphodiesterase 1c, a regulator of Ca^{2+} and cGMP-dependent intracellular
196 signaling. This methylation pattern differed between hippocampus from GM^{Low} and GM^{High} mice, and was
197 conserved between birth dam and offspring, regardless of postnatal colonization (**Fig. 3c**). Similarly,
198 microbiome-associated differences in methylation were identified at multiple closely spaced markers on
199 both strands of chromosome 14, including markers associated with the genes *Ang5* and *Ang6* (**Fig. 3d**),
200 encoding members 5 and 6, respectively, of the angiogenin, ribonuclease A family.
201 To identify shared pathways or commonalities among the functional products (i.e., proteins) encoded by
202 protein-coding genes among the DMRs, a STRING analysis was performed using a final input of 144 gene
203 names. Interaction analysis resulted in assembly of one large network with 32 nodes, a smaller network
204 with six nodes, and four dyads (**Fig. 3e**). While enrichment analysis failed to detect greater network
205 connectivity than would occur at random, stratified analysis of the 32 nodes in the large network
206 revealed 10 significantly enriched Gene Ontology (GO) Biological Processes; five GO Molecular Functions
207 including TGF-β receptor binding (GO:0005160, strength 1.94, FDR-adjusted $p = 0.015$) and GTPase
208 activity (GO:0003924, strength = 1.09, FDR-adjusted $p = 0.042$); five KEGG pathways including Gap
209 junction (mmu04540, strength = 1.38, FDR-adjusted $p = 0.033$) and TGF-β signaling pathway
210 (mmu04350, strength = 1.32, FDR-adjusted $p = 0.033$); and four Reactome pathways including axon
211 guidance (MMU-422475, strength = 1.08, FDR-adjusted $p = 0.048$). Collectively, these data provide
212 evidence suggesting the inheritance of maternal DNA methylation profiles in the fetal hippocampus, in
213 association with differences in the maternal microbiome. The distribution and relationship of genes
214 affected by differential methylation reflects a semi-stochastic effect across the fetal genome, with
215 modest enrichment for genes with broad associations such as TGF-β signaling, GTPase activity, and axon
216 guidance.
217

218 **Fetal programming of gene expression in hippocampus by maternal microbiome**

219 We next performed single nuclei RNAseq on hippocampus collected from control mice and cross-
220 fostered mice. Based on expression of cell-specific markers, 11 cell clusters were identified in the control
221 mice and 24 cell clusters were identified in the cross-fostered mice (**Extended Data Figure 4a-b**). Based
222 on generalized additive regression models, control mice from GM^{Low} and GM^{High} gene expression were
223 compared, and differentially expressed genes (DEGs) within each treatment group were identified
224 (**Supplementary Table 5**). Similarly, mice from CF^{Low} and CF^{High} were examined for DEGs within each cell
225 cluster (**Supplementary Table 6**). After DEGs from each cell cluster had been determined using $Log_2FC >$
226 1.5, STRING analysis was used to determine the protein-protein interactions of the DEGs from each
227 treatment. The number of DEGs from each cell cluster were compared to the mean node degree
228 received from the STRING analysis to determine which cell clusters contained a high number of DEGs
229 that were most likely to interact within protein pathways. Interestingly the cell cluster with the highest
230 number of DEGs, as well as the highest number of mean node degree of protein-protein interactions in
231 both control and cross-foster mice, was identified as endothelial cells (**Extended Data Figure 5a-b**). We
232 then performed STRING analysis to generate interaction networks using DEGs identified in the
233 endothelial cells of control mice as well as the cross-fostered mice (**Fig. 4a-b**). Of these interactions, six
234 DEGs (*Fas, Fzd6, Gja1, Ntng1, Pik3r3, Sox17*) showed a pattern of fetal programming. Of note, numerous
235 DEGs identified were also found among differentially methylated genes or closely related to differentially
236 methylated genes (**Fig. 4b**). When astrocyte and L5 IT glutamatergic neurons were examined using
237 interaction networks, they also contained multiple DEGs that showed a pattern of fetal programming as
238 well as DEGs that were identified as differentially methylated (**Extended Fig. 6a-b, and Extended Data**
239 **Fig. 7a-b**). When we examined the Log_2FC of *Dock1* expression of CF^{Low} and CF^{High}, *Dock1* was shown to
240 be upregulated in the clusters of endothelial cells, oligodendrocyte, microglial cells, and subsets of
241 astrocytes and glutamatergic neurons of CF^{High} mice compared with CF^{Low} (**Fig. 4c**). Similarly, when we
242 examined expression of *Pde1c*, it too was increased in the endothelial cell cluster of CF^{High} mice, though
243 not consistent with the expression patterns of other cells seen with *Dock1* (**Fig. 4d**). We next used
244 CellChat software to examine the cell-cell communication interactions of all DEGs identified in the
245 control groups, and then in the cross-foster groups to identify cell signaling pathways that show a
246 pattern of fetal programming. There were 42 cell-cell communication pathways that were shared
247 between the control mice and the cross-foster mice (**Fig. 4e**). Of the 42 pathways identified, 15 showed a
248 pattern of fetal programming including *Vegf*, *Igf*, *Il2*, *Tgfβ*, *Wnt*, and *Npy* (**Fig. 4f-g**). Interestingly, three
249 cell-cell communication pathways that were identified in only GM^{Low} and CF^{High} were appetite-stimulating

250 orexigenic neuropeptide pathways, giving a possible reason for the increased weight noted in these two
251 groups. These findings highlight cell type-specific differences in hippocampal gene expression in genes
252 identified within DMRs and genes in pathways associated with growth and feeding behavior. In total, the
253 findings presented here demonstrate differentially abundant features within a healthy GM influence
254 behavior, DNA methylation, and gene expression within the central nervous system, and strongly suggest
255 a relationship between these events during fetal development.
256

257 **Methods**

258 **Mice**

259 All activities described here were performed in accordance with the guidelines put forth in the Guide for
260 the Care and Use of Laboratory Animals and were approved by the Institutional Animal Care and Use
261 Committee (IACUC) of the University of Missouri, an AAALAC accredited institution. All mice tested in the
262 current study were outbred CD1 mice generated from breeders colonized with GM^{Low} or GM^{High},
263 originally obtained from the Mutant Mouse Resource and Research Center at the University of Missouri
264 (MU MMRRC). Colonies of mice were housed under barrier conditions in microisolator cages with
265 compressed pelleted paper bedding and nestlets, on ventilated racks with *ad libitum* access to irradiated
266 chow and acidified, autoclaved water, under a 14:10 light/dark cycle. Mice were determined to be free
267 of all bacterial pathogens including *Bordetella bronchiseptica*, *Filobacterium rodentium*, *Citrobacter*
268 *rodentium, Clostridium piliforme, Corynebacterium bovis, Corynebacterium kutscheri, Helicobacter* spp.,
269 *Mycoplasma* spp., *Rodentibacter* spp., *Pneumocystis carinii, Salmonella* spp., *Streptobacillus*
270 *moniliformis, Streptococcus pneumoniae*; adventitious viruses including H1, Hantaan, KRV, LCMV, MAD1,
271 MNV, PVM, RCV/SDAV, REO3, RMV, RPV, RTV, and Sendai viruses; intestinal protozoa including
272 *Spironucleus muris, Giardia muris, Entamoeba muris,* trichomonads, and other intestinal flagellates and
273 amoebae; intestinal parasites including pinworms and tapeworms; and external parasites including all
274 species of lice and mites, via quarterly sentinel testing performed by IDEXX BioAnalytics (Columbia, MO).
275 Fecal samples were collected from pregnant dams at 19 days of gestation, and from mouse pups at time
276 of weaning (21 days of age) using previously described methods[43]. Briefly, mice were placed in an empty
277 autoclaved cage within abiological safety cabinet and allowed to defecate. Freshly evacuated samples
278 feces were immediately collected into a sterile collection tube using autoclaved wooden toothpicks
279 discarded after each single usage. All samples were promptly placed on ice. Following fecal sample
280 collection, samples were stored in a -80°C freezer until DNA extraction was performed. Samples were
281 collected from all experimental mice at 50 days of age, at time of necropsy.

282

283 **Cross-Foster**

284 Mice in cross-foster groups were cross-fostered at less than 24 hours of age to a surrogate dam of the
285 reciprocal GM. Following identification of recently birthed litters from both GMs, cages were moved to a
286 biosafety cabinet. Litters were removed from the cage of the biological dam and placed onto clean paper
287 towels. Bedding from the cage of the surrogate dam was gently mixed with the pups to transfer the
288 surrogate dam's scent to the pups and reduce the possibility of cannibalism. The pups were then placed
289 into the surrogate dam cage, and cages were returned to the appropriate housing rack.

290

291 **Behavior testing**

292 *Open Field Exploration.* The open field exploration test was used to evaluate anxiety-related behavior
293 and locomotor function. Environmental control chambers (Omnitech Electronics, Inc., Columbus, OH)
294 consisting of 4 separate environmental isolation chambers containing a plexiglass box (41cm × 41cm ×
295 30cm) placed onto an infrared grid (41cm × 41cm) to track locomotion. Lighting for each isolation
296 chamber was set to 159 lux. Mice were allowed to acclimate to the behavior room for 1 hour prior to
297 testing. Before starting each test, the plexiglass was cleaned with 0.25% bleach, followed by 70% ethanol
298 to remove any residual olfactory cues. Each mouse was placed into the middle of the open field
299 exploration test and recorded for 30 minutes by the Fusion behavior monitoring software (Omnitech
300 Electronics, Inc., Columbus, OH). The first 20 minutes of the test were considered acclimation time, and
301 the final 10 minutes were analyzed following completion of the test. Total distance traveled (cm), time
302 spent in the center zone (seconds), distance traveled in the center zone, and vertical activity (rearing)
303 were measured.

304 *Light/Dark Transition.* The light/dark transition test was performed within the environmental control
305 chambers (Omnitech Electronics, Inc., Columbus, OH, USA). The apparatus consisted of a plexiglass box
306 within the environmental chambers (41cm × 41cm × 30cm) that were partitioned into two equal sections
307 by a black plexiglass insert with a door that allowed one half to be a dark zone, and a second half to be a
308 light zone. The light zone was illumination was set to 200 lux. Mice were allowed to acclimate to the
309 behavior room for 1 hour prior to testing. Before the start of each test, the plexiglass box and insert were
310 cleaned with 0.25% bleach, followed by 70% ethanol to remove any residual olfactory cues. Mice were
311 placed into the light zone facing away from the dark zone and monitored by Fusion behavior monitoring
312 software (Omnitech Electronics, Inc., Columbus, OH, USA) for 15 minutes. Time spent in the light zone

313 (sec), distance travelled in the light zone (cm), and number of transitions between light and dark zones
314 were measured.
315 *Elevated Plus Maze.* The elevated plus maze test consisted of an apparatus with two open arms (32.5 × 5
316 cm, with 2-mm ledges) and two closed arms (32.5 × 5 cm, with 14.5 cm high walls). The open arms were
317 arranged perpendicular to the closed arms so the apparatus formed the shape of a plus sign with a
318 center square (5 × 5 cm). The entire apparatus was raised 50 cm above the floor. The center zone of the
319 apparatus was illuminated to 50 lux. Mice were allowed to acclimate to the behavior room for 1 hour
320 prior to testing. Prior to testing, the apparatus was cleaned with 0.25% bleach followed by 70% ethanol
321 to remove olfactory cues. Each mouse was placed in the center square facing an open arm and was
322 recorded and monitored for 5 minutes. Distance Traveled in the open arms (cm), time spent in the open
323 arms (sec), and number of entries into the open arms was calculated from distance measurements and
324 entry counts obtained by Any-Maze monitoring software (Stoelting Co., Wood Dale, IL, USA).
325 *Voluntary running.* Litters for running wheel experiments were culled to six pups per litter (3 male, 3
326 female) at birth, and then weaned into same-sex trios at weaning. During wheel set-up at seven weeks
327 of age, mice were transferred from their home cage to a new static microisolator cage containing a
328 wireless running wheel (Med Associates, ENV-047) connected to a wireless hub and laptop computer in
329 the animal room. Mice were singly housed during the experiment, assigned to running wheel cages using
330 a random number generator, and were placed in alternating order on the shelf such that microbiome
331 group and sex were consistently alternated. Following five days of acclimation, data were collected
332 continuously for seven consecutive days using Wheel Manager software, v2.04.00 (Med Associates, SOF-
333 860). Data were analyzed using Wheel Analysis software, v2.02.01 (Med Associates, SOF-861). No other
334 mice were housed in the room containing running wheels, traffic was limited to daily checks by
335 laboratory staff, and no cage changes were performed during the acclimation and test period.
336
337 **Necropsy**
338 Mice were transported to the necropsy room at 50 days of age, and allowed to acclimate to the room for
339 1 hour. Mice were then euthanized one at a time by CO_2 asphyxiation out of sight of other mice. The
340 euthanasia chamber was cleaned with 70% ethanol between mice to eliminate olfactory cues. Following
341 loss of paw pinch and righting reflexes, blood was collected by cardiac puncture and placed into serum
342 separator tubes. The brain was then removed, and the hippocampus was gently dissected out, placed in
343 a 2 mL tube, and promptly plunged into liquid nitrogen to flash freeze. Liver and ileum were isolated,
344 placed in a 2mL tube, and promptly plunged into liquid nitrogen. Two fecal pellets collected from the

345 colon for 16S rRNA gene analysis. Blood was allowed to clot for 30 minutes at room temperature, and
346 was then centrifuged at 4,000 RPM for 15 minutes, and serum placed into a 1.5 mL microcentrifuge
347 tube. Hippocampus, feces, and serum were promptly placed into -80°C freezer for storage.
348
349 **Metabolite analyses**

350 *GC-MS.* Fecal and plasma samples were diluted in 18 volumes of ice-cold 2:2:1
351 methanol/acetonitrile/water containing a mixture of internal standards (D4-citric acid, D4-succinic acid,
352 D8-valine, and U13C-labeled glutamine, glutamic acid, lysine, methionine, serine, and tryptophan;
353 Cambridge Isotope Laboratories), where the 1-part water was composed of sample volume + water.
354 Sample extraction mixtures were vortexed for 10 minutes at RT and rotated for 1 hour at -20°C.
355 Mixtures were centrifuged for 10 minutes at 21,000 × g, and 150 µL of the cleared metabolite extracts
356 were transferred to autosampler vials and dried using a SpeedVac vacuum concentrator (Thermo). Dried
357 metabolite extracts were reconstituted in 30 µL of 11.4 mg/mL methoxyamine (MOX) in anhydrous
358 pyridine, vortexed for 5 minutes, and heated for 1 hour at 60°C. Next, to each sample 20 µL of N,O-
359 Bis(trimethylsilyl)trifluoroacetamide (TMS) was added, samples were vortexed for 1 minute, and heated
360 for 30 minutes at 60°C. Derivatized samples were analyzed by GC-MS. One µL of derivatized sample was
361 injected into a Trace 1300 GC (Thermo) fitted with a TraceGold TG-5SilMS column (Thermo) operating
362 under the following conditions: split ratio = 20:1, split flow = 24 µL/minute, purge flow = 5 mL/minute,
363 carrier mode = Constant Flow, and carrier flow rate = 1.2 mL/minute. The GC oven temperature gradient
364 was as follows: 80°C for 3 minutes, increasing at a rate of 20°C/minute to 280°C, and holding at a
365 temperature at 280°C for 8 minutes. Ion detection was performed by an ISQ 7000 mass spectrometer
366 (Thermo) operated from 3.90 to 21.00 minutes in EI mode (-70eV) using select ion monitoring (SIM).

367 *LC-MS SCFA analysis.* 18-fold (w/v) extraction solvent (Acetonitrile:Methanol:Water (2:2:1)) containing
368 deuterated SCFA standards (D3-acetate, D7-butyrate, and D5-propionate) was added to each sample
369 and rotated at -20°C for 1 hr and then centrifuged at 21,000 × g for 10 min. Supernatant was used for
370 LC-MS SCFA analysis. LC-MS data was acquired on a Thermo Q Exactive hybrid quadrupole Orbitrap mass
371 spectrometer with a Vanquish Flex UHPLC system or Vanquish Horizon UHPLC system. The LC column
372 used was a ZIC-pHILIC guard column (20 × 2.1 mm). The injection volume was 2 µL. For the Mobile
373 phase, Solvent A consisted of 20 mM ammonium carbonate [(NH4)2CO3] and 0.1% ammonium
374 hydroxide (v/v) [NH4OH] at pH ~9.1] and Solvent B consisted of Acetonitrile. This method was run at a
375 flow rate of 0.1 mL/min, and the injection volume was 2 µL. Linear gradient was used at 70% solvent B

376 with a 5 min elution time. The mass spectrometer was operated in targeted selected ion-monitoring
377 (tSIM) mode from 1 to 5 minutes. An inclusion list for the three short chain fatty acids and their
378 deuterated versions were used in tSIM method.

379 *LC-MS bile acid analysis.* Extraction solvent (methanol:acetonitrile:water, 2:2:1) was spiked with (5
380 µLI/mL) deuterated bile acids MaxSpec Mixture (Cayman Chemicals Item no. 33506). 18-fold volume
381 extraction buffer was added to each sample. The samples were placed in a -20°C freezer for 1 hour while
382 rotating. The samples were then centrifuged at 21,000 × g for 10 minutes. Supernatant was transferred
383 to LC-MS autosampler vials for analysis. LC-MS data was acquired on a Thermo Q Exactive hybrid
384 quadrupole Orbitrap mass spectrometer with a Vanquish Flex UHPLC system or Vanquish Horizon UHPLC
385 system. A Thermo Hypersil GOLD (2.1 × 150 mm, 1.9 µm) UHPLC column was used with a column
386 Temperature of 30°C. For the Mobile Phase, solvent A consisted of 1% acetonitrile in water with 0.1%
387 formic acid, and solvent B is 99% acetonitrile with 0.1% formic acid. The gradient started at 50% Solvent
388 B and was held for 2.5 minutes; then increased to 100% B at 10 minutes and held for 0.5 minutes before
389 re-equilibration to 50% solvent B for 5.5 min. Flow Rate was 0.4 mL/min, and injection volume was 3 µL.
390 The mass spectrometer was operated in full-scan negative mode, with the spray voltage set to 3.0 kV,
391 the heated capillary held at 275°C, and the HESI probe held at 350°C. The sheath gas flow was set to 40
392 units, the auxiliary gas flow was set to 15 units, and the sweep gas flow was set to 1 unit. MS data
393 acquisition was performed in a range of m/z 70–1,000, with the resolution set at 70,000, the AGC target
394 at 1 × 106, and the maximum injection time at 200 ms.[44].

395 *Metabolomic Data Analysis.* GC-MS Raw data were analyzed using TraceFinder 5.1 (Thermo). Metabolite
396 identification and annotation required at least two ions (target + confirming) and a unique retention
397 time that corresponded to the ions and retention time of a reference standard previously determined
398 in-house. A pooled-sample generated prior to derivatization was analyzed at the beginning, at a set
399 interval during, and the end the analytical run to correct peak intensities using the NOREVA tool[45].
400 NOREVA corrected data were then normalized to the total signal per sample to control for extraction,
401 derivatization, and/or loading effects. Acquired LC-MS data were processed by Thermo Scientific
402 TraceFinder 4.1 software, and metabolites were identified based on the University of Iowa
403 Metabolomics Core facility standard-confirmed, inhouse library. NOREVA was used for signal drift
404 correction[45]. For bile acids, data were normalized to one of the d4-bile acid standards. For SCFA, analyte
405 signal was corrected by normalizing to the deuterated analyte signal and the signal obtained from
406 processing blank was subtracted.

407

408 **Microbiome analysis**

409 *DNA extraction*. Fecal DNA was extracted using QIAamp PowerFecal Pro DNA kits (Qiagen), according to
410 the manufacturer's instructions, with the exception that the initial sample disaggregation was performed
411 using a TissueLyser II (Qiagen), rather than a vortex and adaptor as described in the protocol.

412 *16S rRNA amplicon library preparation and sequencing*. Extracted fecal DNA was processed at the
413 University of Missouri DNA Core Facility. Bacterial 16S rRNA amplicons were constructed via
414 amplification of the V4 region of the 16S rRNA gene using previously developed universal primers
415 (U515F/806R), flanked by Illumina standard adapter sequences[46, 47]. Oligonucleotide sequences are
416 available at proBase[48]. Dual-indexed forward and reverse primers were used in all reactions. PCR was
417 performed in 50 µL reactions containing 100 ng metagenomic DNA, primers (0.2 µM each), dNTPs (200
418 µM each), and Phusion high-fidelity DNA polymerase (1U, Thermo Fisher). Amplification parameters
419 were $98°C^{(3\ min)}$ + [$98°C^{(15\ sec)}$ + $50°C^{(30\ sec)}$ + $72°C^{(30\ sec)}$] × 25 cycles + $72°C^{(7\ min)}$. Amplicon pools (5
420 µL/reaction) were combined, thoroughly mixed, and then purified by addition of Axygen Axyprep
421 MagPCR clean-up beads to an equal volume of 50 µL of amplicons and incubated for 15 minutes at room
422 temperature. Products were washed multiple times with 80% ethanol and the dried pellet was
423 resuspended in 32.5 µL EB buffer (Qiagen), incubated for two minutes at room temperature, and then
424 placed on a magnetic stand for five minutes. The final amplicon pool was evaluated using the Advanced
425 Analytical Fragment Analyzer automated electrophoresis system, quantified using quant-iT HS dsDNA
426 reagent kits, and diluted according to Illumina's standard protocol for sequencing on the MiSeq
427 instrument.

428 *Bioinformatics*. DNA sequences were assembled and annotated at the MU Informatics Research Core
429 Facility. Primers were designed to match the 5' ends of the forward and reverse reads. Cutadapt[49]
430 (version 2.6) was used to remove the primer from the 5' end of the forward read. If found, the reverse
431 complement of the primer to the reverse read was then removed from the forward read as were all
432 bases downstream. Thus, a forward read could be trimmed at both ends if the insert was shorter than
433 the amplicon length. The same approach was used on the reverse read, but with the primers in the
434 opposite roles. Read pairs were rejected if one read or the other did not match a 5' primer, and an error-
435 rate of 0.1 was allowed. Two passes were made over each read to ensure removal of the second primer.
436 A minimal overlap of three bp with the 3' end of the primer sequence was required for removal. The
437 QIIME2[50] DADA2[51] plugin (version 1.10.0) was used to denoise, de-replicate, and count ASVs (amplicon
438 sequence variants), incorporating the following parameters: 1) forward and reverse reads were

439 truncated to 150 bases, 2) forward and reverse reads with number of expected errors higher than 2.0
440 were discarded, and 3) Chimeras were detected using the "consensus" method and removed. R version
441 3.5.1 and Biom version 2.1.7 were used in QIIME2. Taxonomies were assigned to final sequences using
442 the Silva.v132[52] database, using the classify-sklearn procedure.
443
444 **Real-time reverse transcription-polymerase chain reaction (qRT-PCR)**
445 Total RNA was isolated from tissues using the Qiagen RNeasy Mini Kit per manufacturer's instructions.
446 RT-PCR was performed using the BioRad iTaq Universal SYBR Green One-Step Kit following the
447 manufacturers instructions. Briefly, each reaction consisted of 5µL of SYBR Green Supermix, 0.125µL
448 iScript reverse transcriptase, 0.45µL of forward and reverse primers, 1.475µL of water, and 2.5µL of
449 template RNA. The reaction was run on a BioRad C1000 Touch thermal cycler with a BioRad CFX384 Real-
450 Time System with the following parameters: 50˚C for 10 min for reverse transcription, 95˚C for 1 min for
451 DNA Polymerase activation and DNA denaturation, and 40 cycles of 95˚C for 10 sec and 60˚C for 30 sec.
452 Melt-curve analysis was performed using the following parameters: 65-95˚C with 0.5˚C increments for 5
453 sec/step. Primers used can be found in **Supplementary Table 7**.
454
455 **Bile salt hydrolase metagenomic and metatranscriptomic analysis of mouse feces**
456 Metagenomic and metatranscriptomic *bsh* (K01442) read counts were acquired from previous multi-
457 omic analysis of GM^{Low} (GM1) and GM^{High} (GM4)[53]. Expression counts from metatranscriptomic analysis
458 were normalized to *bsh* metagenomic reads.
459
460 **Measurement of BSH activity in mouse feces**
461 BSH activity in the mouse feces was measured using previously reported bioluminescent bile acid
462 activatable luciferin probes (BAL) protocol[54] with major modification by replacing whole-cell
463 bioluminescence readout with the recombinant luciferase enzymatic assay[55]. Mouse fecal samples were
464 soaked in PBS (pH 7.4, Gibco, ref# 10010-023) supplemented with 2-mercaptoethanol (Acros Organics,
465 20 mM) at a concentration of 10 mg/mL on ice for 30 min. The mixtures were homogenized by
466 sonication in ultrasound cleaner (Elmasonic Easy 40 H, 340 W) at 0°C for 30 min, stirring every 10 min.
467 Resulting mixtures along with blank buffer (3 replicates by 50 µL) were mixed with working solutions of
468 BAL probes (50 µL, 20 µM in PBS) along with a solution of luciferin (50 µL, 2 µM in PBS) in a 96-well assay
469 plate (Corning, ref# 3595) and incubated at 37°C for 1 h. After incubation, the mixtures were diluted with
470 2% Triton X-100 in PBS (100 µL) to stop the reaction. In a separate 96-well flat bottom black plate

471 (Corning, ref# 3650), resulting mixtures (5 µL) were diluted with PBS (50 µ). A luciferase solution
472 containing recombinant luciferase from Photinus pyralis (Sigma-Aldrich, 20 µg/mL), ATP disodium
473 trihydrate (Fisher Scientific, 2 mM), and magnesium sulfate heptahydrate (Fisher Scientific, 2 mM) in PBS
474 (50 µL) was added to each well simultaneously. Bioluminescence was measured immediately in an IVIS
475 Spectrum (Xenogen) imaging system for 20 min with 1 min intervals using automatic settings. Raw data
476 were processed using Living Image 4.2 software (Caliper LifeSciences), further data processing was
477 carried out in Excel (Microsoft 365), and finally visualization and statistical calculations were performed
478 in Prism 9 (GraphPad software). Deconjugation potentials or percentage of probe hydrolysis were
479 calculated as the ratio of the signal from the BAL probe to the signal from luciferin in the corresponding
480 fecal extract and reported as the mean value of 3 replicates. The signals from incubation of BAL probes in
481 blank buffer provided a background result of nonspecific hydrolysis of the probes.
482
483 **Isolation of hippocampal nuclei**
484 Single nuclei were isolated from mouse hippocampal tissue samples as follows. Briefly, Nuclei Lysis
485 Buffer was prepared by adding 12 mL of Nuclei EZ Prep Lysis Buffer (Sigma-Aldrich, St. Louis, MO, USA) to
486 a 15mL tube and adding 1 cOmplete Ultra tablet (Sigma-Aldrich, St. Louis, MO, USA) and allowing tablet
487 to dissolve. Two 4-mL aliquots of the Nuclei EZ Prep Lysis Buffer + cOmplete Ultra tablets were then
488 placed in 15 mL tubes. Twenty (20) µL of Protector RNase inhibitor (Sigma-Aldrich, St. Louis, MO, USA)
489 and 20uL of Superase-In (MilliporeSigma, Burlington, MA, USA) were added to one 4 mL aliquot to make
490 Nuclei Lysis Buffer 1 (NLB1). Four (4) µL of Protector RNase inhibitor (Sigma-Aldrich, St. Louis, MO, USA)
491 and 4 µL of Superase-In (MilliporeSigma, Burlington, MA, USA) were added to the second -mL aliquot to
492 make Nuclei Lysis Buffer 2 (NLB2). Suspension Buffer (SB) was prepared by adding 1 mL of fetal bovine
493 serum (Sigma-Aldrich, St. Lous, MO, USA) to 9 mL of 1× phosphate-buffered saline with 4 µL of Protector
494 RNase inhibitor (Sigma-Aldrich, St. Louis, MO, USA). Eight (8) hippocampi halves from eight individual
495 mice were pooled and homogenized to a single cell suspension in a 2 mL dounce homogenizer with 2 mL
496 of NBL1. The sample was then strained through a 200 µm strainer (pluriSelect Life Science, El Cajon, CA,
497 USA) and the strained cell suspension returned to the 2 mL dounce and homogenized to a nuclei
498 suspension. The nuclei were strained through a 40 µm strainer (pluriSelect Life Science, El Cajon, CA,
499 USA) and centrifuged at 500 RCF at 4°C for 5 minutes. Supernatant was removed, and pellet was
500 resuspended with NLB2 and incubated at 4°C for 5 minutes. Nuclei were then centrifuged at 500 RCF at
501 4°C for 5 minutes, supernatant was removed, and nuclei were resuspended in suspension buffer.
502

503 **10x Genomics single cell 3' RNA-Seq library preparation**

504 Libraries were constructed by following the manufacturer's protocol with reagents supplied in 10x
505 Genomics Chromium Next GEM Single Cell 3 Kit v3.1. Briefly, nuclei suspension concentration was
506 measured with an Invitrogen Countess II automated cell counter. Nuclei suspension (1,200 nuclei per
507 microliter), reverse transcription master mix, and partitioning oil were loaded on a Chromium Next GEM
508 G chip with a nuclei capture target of 8,000 nuclei per library. Post-Chromium controller GEMs were
509 transferred to a PCR strip tube and reverse transcription performed on an Applied Biosystems Veriti
510 thermal cycler at 53°C for 45 minutes. cDNA was amplified for 13 cycles and purified using Axygen
511 AxyPrep MagPCR Clean-up beads. Fragmentation of cDNA, end-repair, A-tailing and ligation of
512 sequencing adaptors was performed according to manufacturer specifications. The final library was
513 quantified with the Qubit HS DNA kit and the fragment size determined using an Agilent Fragment
514 Analyzer system. Libraries were pooled and sequenced on an Illumina NovaSeq 6000 to generate 50,000
515 reads per nuclei.

516

517 **Single cell bioinformatics**

518 FASTQ files were generated from the raw base call outputs using Cell Ranger (10X Genomics) pipeline,
519 *mkfastq* v3.0. Using default parameters, a UMI (gene-barcode) count matrix per sample was obtained
520 using the built-in Cell Ranger count pipeline. To reduce noise, we only kept genes that were detected in
521 at least three barcodes, and subsequently removed ribosomal-encoded genes from the count matrix.
522 Scrublet[56] was then used to identify potential multiplet-barcodes and only those with a doublet score of
523 less than 0.15 were used for downstream analyses. The files were then combined in a single embedding
524 for the control and CF groups separately, following the Seurat v3 integration workflow[57]. SCTransform
525 was used to normalize each sample, followed by the identification of integration anchors and variable
526 features using the Seurat workflow. Dimension reduction was performed scaled data after 4000 highly
527 variable genes across the samples were identified (*SelectIntegrationFeatures* function). The
528 *IntegrateData* function was then used to obtain a combined and centered matrix, where the top 30
529 components were used to carry out ordination analyses. These components were used to build a SNN
530 (shared nearest neighbour) graph which was subsequently clustered using the *Louvain* algorithm for
531 speed and computational efficiency. The principal components were then mapped into two dimensions
532 using the default uniform manifold approximation and projection (UMAP) algorithm, where the n = 30
533 neighbours was set, with a minimum distance of 0.4. Finally, the *FindAllMarkers* function was used to
534 identify marker genes for each cluster. The top marker genes were used manually based on literature

535 searches to assign cell type annotations for each cluster. This was further corroborated by cluster
536 annotations using the Azimuth mouse reference datasets[57]. The cell types across samples and groups
537 were combined with their pseudo bulk profiles, and the resulting gene-cell type matrix was normalized
538 by estimating transcripts per million and transformed (log2) for downstream analyses. To obtain
539 statistically enriched differential gene expression, we used generalized additive regression models,
540 where in the control or CF variables, alongside the GM^{Low} or GM^{High} status were encoded as independent
541 variables. The models were analyzed for each cluster independent of the other, where per gene log2
542 fold-change was determined. Significance was identified as those genes with an adjusted p-value of less
543 than 0.05, following Benjamini-Hochberg correction. All figures and statistical analyses were performed
544 using R v4.1[58].
545 Cell-to-cell communication was inferred using log10-transformed gene expression data collected from
546 snRNA-seq of the mouse hippocampus using CellChat[59, 60]. Cell clusters as identified above were grouped
547 into the following cell types based on Azimuth classification: Glutamatergic and GABAergic neurons,
548 Periendothelial Cells, Microglia, Astrocytes, and Oligodendrocytes. Ligand-receptor interactions were
549 inferred using the mouse reference database provided by CellChat (Accessed May 25, 2023).
550 Overexpressed genes and interactions were determined using default settings. Cell-cell communication
551 probability was inferred using default settings. Information flow was determined by the summation of
552 communication probability for each pathway.
553
554 **Methylome analysis**
555 Hippocampal genomic DNA was isolated from adult female cross-foster (CF) and control (non-CF)
556 offspring samples using the DNAeasy kit (Qiagen, Valencia, CA) following the manufacturer's
557 instructions. For studying Genome-wide DNA methylation profiles, 1 µg of genomic DNA was treated
558 with sodium bisulfite (Zymo Research, Irvine, CA). Converted DNA was analyzed using Infinium Mouse
559 Methylation BeadChip assay (Illumina, San Diego, CA). This array includes over 285,000 CpG sites
560 covering all RefSeq genes, including CpG islands, translation start sites, enhancers, imprinted loci, and
561 other regions[61]. All data analyses were conducted using the R environment version 4.2.0. Microarray
562 data was processed using the *ENmix* version.1.34.02[62] and *minfi* v.1.44.0[63] packages. Quantile
563 normalization of U or M intensities for Infinium I or II probes were performed, respectively. A model-
564 based correction was performed, and a dye-bias correction was conducted using *RELIC* [64]. β-values
565 representing the averaged total intensity value per CG position was calculated as unmethylated intensity
566 (U) + methylated intensity (M) [M / (U + M + 100)]. Probes with a detection $p < 1 \times 10^{-6}$ and less than 3

567 beads were defined as low quality. Samples with low quality methylation measurements > 5% or low
568 intensity bisulfite conversion probes were removed from further analysis. Differentially methylated
569 positions (DMPs) between the experimental groups were determined using the *ENmix* version.1.34.02[62]
570 package. For each position, the magnitude of the DNA methylation difference was expressed as Fold
571 Changes in the logarithmic scale (logFC) and the significance of the difference as a FDR-corrected p-Value
572 (q value).

573

574 **Statistics**

575 Two-way ANOVA followed by Tukey's post-hoc analysis was used to compare differences in groups across
576 all behavior testing parameters. Specific parameters analyzed included time spent in center zone,
577 distance travelled in center zone, total distance travelled (OFE), time spent in light chamber, distance
578 travelled in light chamber, number of entries into light chamber (LDT), and time spent in open arms,
579 distance travelled in open arms, number of entries into open arms (EPM). All univariant data analysis
580 was performed using SigmaPlot 14.0 (Systat Software, Inc, San Jose, CA). For multivariate data (e.g.,
581 microbiome beta-diversity), two-way permutational multivariant analysis of variance (PERMANOVA) was
582 used with main effects of age and GM. PERMANOVA analysis was performed using the PAST 4.03
583 software and was based on Bray-Curtis dissimilarities. All diversity and richness indices were calculated
584 using PAST 4.03 software, followed by two-way ANOVA for main affects of age and GM using SigmaPlot
585 14.0 (Systat Software, Inc, San Jose, CA). Due to uniform lack of normality across metabolites, a Mann-
586 Whitney U test was used to test for statistical differences in metabolite concentrations between
587 treatment groups.

588

589 **Statement of data availability**

590 All data supporting our analyses and reported conclusions have been deposited in the appropriate data
591 repositories and are publicly available. Metagenomic, metatranscriptomic, and 16S rRNA amplicon
592 sequencing data are available at the National Center for Biotechnology and Informatics (NCBI) Sequence
593 Read Archive (SRA) under the BioProject accession number PRJNA885816. Mouse Methylation
594 BeadChip array data are available at the Gene Expression Omnibus (GEO) under accession GSE239371.

595

596 **Acknowledgements**

The authors would like to acknowledge the University of Iowa Metabolomics Core Facility, the University of Missouri Mutant Mouse Resource and Research Center, the University of Missouri Metagenomics Center, and the University of Missouri Office of Animal Resources.

Figure legends

Figure 1. Anxiety-related behavior and other outcomes in offspring are influenced by the maternal gut microbiome. a. Schematic showing the experimental groups and timing of outcome measures. **b-e.** Behavior outcomes in male (M) and female (F) mice colonized with GM^{Low} or GM^{High}, including time spent in the light portion of a light/dark test (**b**), time spent in the open arms of an elevated plus maze (**c**), and distance run per day (Km) by male (**d**) and female (**e**) mice. **f.** Body weight per mouse (grams) at day 50 in control mice. **g-j.** Same behavior outcomes in CF^{Low} and CF^{High} mice as those shown in panels **b-e**. **k.** Body weight per mouse at day 50 in cross-fostered mice. p and F values represent effect of GM in two-way ANOVA with Tukey post hoc. Significant sex-dependent differences were detected in distance on running wheels and body weight in both control and cross-fostered mice, with no significant interactions between GM and sex in any tests. * $p<0.05$, ** $p<0.01$, **** $p<0.0001$

Figure 2. Microbiomes linked to fetal programming of complex behaviors differ in synthesis or catabolism of several metabolites including bile acids. a. Hierarchical clustering of data from adult GM^{Low}- or GM^{High}-colonized mice, demonstrating segregation of GMs by richness and composition (legend at right). **b,c.** Volcano plots showing metabolites enriched in GM^{Low} (red dots) or GM^{High} (blue dots) feces (**b**) or serum (**c**). **d-g.** Normalized ileal expression of *Asbt* (**d**), *Ostβ* (**e**), *Gpbar1* (**f**), and *Fxr* (**g**) male (M) and female (F) mice colonized with GM^{Low} (red dots) or GM^{High} (blue dots). **j.** Normalized hepatic expression of *Cyp7a1* (**h**), *Slc10a1* (**i**), and *S1pr2* (**j**) in the same groups of mice. Gene expression normalized to *β-Actin* expression. Results indicate main effect of GM in one- or two-way ANOVA, following correction for multiple tests. * $p<0.05$, ** $p<0.01$, **** $p<0.0001$. Abbreviations: 2-HBA (2-hydroxybutyrate), α-MCA (alpha-Muricholic Acid), β-ALA (beta-Alanine), BUTY (Butyrate), CA (Cholic Acid), CDCA (Chendeoxycholic Acid), CYS (Cysteine), DCA (Deoxycholic Acid), F6P (Fructose-6-Phosphate), G6P (Glucose-6-Phosphate), GCA (Glycocholic Acid), GLY (Glycerate), INO (Inositol), LAC (Lactate), LEU (Leucine), MVA (Mevalonic Acid), R5P (Ribulose-5-Phosphate), SUC (Succinate), TCA (Taurocholic Acid), TCDCA (Taurochenodeoxycholic Acid), TDCA (Taurodeoxycholic Acid), TLCA (Taurolithocholic Acid), UDCA (Ursodeoxycholic Acid).

627 **Figure 3. Maternal microbiome is associated with gene methylation in offspring hippocampus. a.** Dot
628 plot showing normalized difference [Log_2(FC)] in mean methylation between GM^{Low} and GM^{High}, and
629 between CF^{Low} and CF^{High}, of all CpG markers achieving a Log_2(FC) > 1 in either comparison. **b.** Ratio of
630 observed to predicted differentially methylated regions (DMRs), and locations of DMRs relative to gene
631 bodies, on each chromosome. **c.** Mean beta values of 27 CpG sites spanning the enhancers, promoters,
632 introns and exons across the *Pde1c* gene in all four groups, with specific sites indicated above (upper);
633 and log_2(FC) between control and cross-fostered groups (lower). **d.** Mean beta values (upper) and
634 Log_2(FC) between groups (lower) across adjacent regions of the positive (left) and negative (right) strand
635 of a region of chromosome 14 containing genes for *Ang5*, *Ang6*, and other genes. **e.** Protein interaction
636 networks among products of DMRs, with node color indicating Log_2(FC) in methylation between GM^{Low}
637 and GM^{High}.

638 **Figure 4. a, b.** Interaction networks constructed using differentially expressed genes (DEGs) identified in
639 hippocampal endothelial and perivascular cells of control (**a**) and cross-fostered (**b**) mice. Highlighted
640 nodes include DEGs identified in both comparisons and showing a pattern of fetal imprinting, and genes
641 that are also differentially methylated (*Pde1c*, *Dock1*), or closely related (PDE cluster, *Dcc*, *Elmo1*, *Dock4*,
642 *Dock5*). **c, d.** Log_2FC in expression of Pde1c (**c**) and Dock1 (**d**) in hippocampal cell clusters of male and
643 female CF^{Low} and CF^{High} mice, as determined via real-time snRNAseq. **e.** Venn diagram showing number of
644 inferred cell-to-cell communication pathways identified in hippocampus of GM^{Low}, GM^{High}, CF^{Low}, and
645 CF^{High} mice. Pathways listed above and below the diagram were selectively identified in the indicated
646 groups. **f, g.** Bar charts showing the relative degree of cell-to-cell communication between GM^{Low} and
647 GM^{High} (**f**), and CF^{Low}, and CF^{High}, (**g**) mice in the indicated pathways.
648

649 **Extended Data**

650 **Extended Data Figure 1. a-e.** Dot and bar plots showing other results of behavior tests in adult male (M)
651 and female (F) GM^{Low} and GM^{High} mice including total distance traveled (**a**) and time spent in the center
652 zone (**b**) during OFE, and distance traveled in the light portion of the light/dark test (**c**) or open arms of
653 the elevated plus maze (**d**), and body weight at 21 days of age (**e**). f-j. Same outcomes in CF^{Low} and CF^{High}
654 mice as those shown in panels **a-e**. * $p<0.05$, ** $p<0.01$, **** $p<0.0001$

655 **Extended Data Figure 2.** Dot and bar plots showing differences in richness (**a**) and principal coordinate
656 analysis (PCoA) plots showing differences in beta-diversity based on Jaccard (**b**) and Bray-Curtis distances
657 (**c**), between adult male (M) and female (F) mice colonized with GM^{Low} or GM^{High}, and similarities in all of

658 the above metrics between CF mice at seven weeks of age and their cognate birth dams. **d.** Cladogram
659 showing results of differential abundance (DA) testing, performed in parallel using ALDEx2 and ANCOM-
660 BC2. Concentric rings at periphery indicate significant DA with enrichment indicated by color (legend
661 upper right) using ALDEx2 (outer); ANCOM-BC2, which first identifies DA based on structural zeros (SZ)
662 or sequences that are absent from one group (middle); and phylum (inner, legend at right). ****
663 p<0.0001

664 **Extended Data Figure 3.** Volcano plots showing the metabolites enriched in feces of GM^{Low}(red dots) and
665 GM^{High} (blue dots) males (**a**), and females (**b**). Volcano plots showing the metabolites enriched in serum
666 of GM^{Low}(red dots) and GM^{High} (blue dots) males (**c**), and females (**d**) and Dot plots representing gene (**e**)
667 and transcript (**f**) copy numbers specific for bile salt hydrolase (Bsh), and the normalized
668 (transcript/gene) expression (**g**) in the feces of adult female mice colonized with GM^{Low} or GM^{High} (*n* =
669 3/GM). Box plots and individual data showing hydrolytic activity of bile salt hydrolase (BSH) in adult male
670 and female mice colonized with GM^{Low} or GM^{High}, determined using five different bile acid-conjugated
671 bioluminescent probes specific for cholic acid (CA, **h**), deoxycholic acid (DCA, **i**), chenodeoxycholic acid
672 (CDCA, **j**), ursodeoxycholic acid (UDCA, **k**), and lithocholic acid (LCA, l). * p<0.05, **** p<0.0001.
673 Abbreviations: 2-HGA (2-hydroxygluterate), 3-HPA (3-Hydroxyproprionate), α-KGA (alpha-Ketogluterate),
674 α-KIC (alpha-Ketoisocaproate), ASP (Asparagine), β-ALA (beta-Alanine), CDCA (Chendeoxycholic Acid),
675 CYS (Cysteine), DCA (Deoxycholic Acid), F6P (Fructose-6-Phosphate), G6P (Glucose-6-Phosphate), GLY
676 (Glycerate), IAA (Indoleacetic Acid), ISO (Isocitrate), LAC (Lactate), LCA (Lithocholic Acid), LEU (Leucine),
677 MAL (Malate), MET (Methionine), ORN (Ornithine), PHEN (Phenylalanine), PRO (Proline), PTA
678 (Pantothenic Acid), R5P (Ribulose-5-Phosphate), SUC (Succinate), TDCA (Taurodeoxycholic Acid), TRY
679 (Tryptamine), VAL (Valine).

680 **Extended Data Figure 4.** UMAP projections of hippocampal cell clusters in control GM^{Low} (**a**) and GM^{High}
681 (**b**), and cross-foster CF^{Low} (**c**) and CF^{High} (**d**) mice.

682 **Extended Data Figure 5. a, b.** Dot plot correlation between the number of differentially expressed genes
683 (DEGs) and the mean node degree determined by protein interaction analysis of those DEGs, in
684 comparisons of GM^{Low} and GM^{High} offspring (**a**) and in CF^{Low} and CF^{High} offspring (**b**). Marker shapes
685 denote cell type including endothelial/perivascular cells (Endo, red squares); astrocytes and
686 oligodendrocytes (Glial, grey diamonds); GABAergic neurons (GABA, dark blue triangles); and
687 glutamatergic neurons (Gluta, brown triangles).

688 **Extended Data Figure 6. a, b.** Interaction networks constructed using differentially expressed genes
689 (DEGs) identified in hippocampal level five intratelencephalon (L5 IT)-projecting glutamatergic neurons
690 from control (**a**) and cross-fostered (**b**) mice. Labeled nodes include DEGs identified in both comparisons
691 and showing a pattern of fetal imprinting, and genes that are also differentially methylated (*Dock1*), or
692 closely related (PDE cluster, *Adcy8*, *Dcc*, *Ntn1*).

693 **Extended Data Figure 7. a, b.** Interaction networks constructed using differentially expressed genes
694 (DEGs) identified in hippocampal astrocyte subsets from control (**a**) and cross-fostered (**b**) mice. Labeled
695 nodes include DEGs identified in both comparisons and showing a pattern of fetal imprinting, and genes
696 that are also differentially methylated (*Dock1*), or closely related (PDE cluster, *Adcy8*, *Dcc*, *Ntn1*).

697

698 **Supplementary Table 1.** Enriched bacterial family taxa harbored by either GM^{Low} or GM^{High}.

699 **Supplementary Table 2.** Results of fecal metabolite concentrations from GM^{Low} and GM^{High} mice.

700 **Supplementary Table 3.** Results of serum metabolite concentrations from GM^{Low} and GM^{High} mice.

701 **Supplementary Table 4.** Differentially methylated regions identified within the genomes of female GM^{Low}
702 and GM^{High} mouse hippocampi.

703 **Supplementary Table 5.** Differentially expressed genes identified within the hippocampal cells of GM^{Low}
704 and GM^{High} control mice.

705 **Supplementary Table 6.** Differentially expressed genes identified within the hippocampal cells of CF^{Low}
706 and CF^{High} mice.

707 **Supplementary Table 7.** Primer pairs used for qRT-PCR analysis**.**

708

709 1. Prevention CfDCa. Anxiety and depression in children: Get the facts. Children's Mental Health.
710 Volume 2023: cdc.gov, 2023.
711 2. Prevention CfDCa. Prevalence of Childhood Obesity in the United States. Overweight and
712 Obesity. Volume 2023. cdc.gov, 2023.
713 3. Gariepy G, Nitka D, Schmitz N. The association between obesity and anxiety disorders in the
714 population: a systematic review and meta-analysis. Int J Obes (Lond) 2010;34:407-19.
715 4. Grundy A, Cotterchio M, Kirsh VA, Kreiger N. Associations between anxiety, depression,
716 antidepressant medication, obesity and weight gain among Canadian women. PLoS One
717 2014;9:e99780.
718 5. Lindberg L, Hagman E, Danielsson P, et al. Anxiety and depression in children and adolescents
719 with obesity: a nationwide study in Sweden. BMC Med 2020;18:30.
720 6. Sharafi SE, Garmaroudi G, Ghafouri M, et al. Prevalence of anxiety and depression in patients
721 with overweight and obesity. Obesity Medicine 2020;17:1-5.

722 7. Wang S, Sun Q, Zhai L, et al. The Prevalence of Depression and Anxiety Symptoms among
723 Overweight/Obese and Non-Overweight/Non-Obese Children/Adolescents in China: A
724 Systematic Review and Meta-Analysis. Int J Environ Res Public Health 2019;16.
725 8. Bercik P, Denou E, Collins J, et al. The intestinal microbiota affect central levels of brain-derived
726 neurotropic factor and behavior in mice. Gastroenterology 2011;141:599-609, 609 e1-3.
727 9. Bravo JA, Forsythe P, Chew MV, et al. Ingestion of Lactobacillus strain regulates emotional
728 behavior and central GABA receptor expression in a mouse via the vagus nerve. Proc Natl Acad
729 Sci U S A 2011;108:16050-5.
730 10. Buffington SA, Di Prisco GV, Auchtung TA, et al. Microbial Reconstitution Reverses Maternal Diet-
731 Induced Social and Synaptic Deficits in Offspring. Cell 2016;165:1762-1775.
732 11. Hsiao EY, McBride SW, Hsien S, et al. Microbiota modulate behavioral and physiological
733 abnormalities associated with neurodevelopmental disorders. Cell 2013;155:1451-63.
734 12. Catron TR, Swank A, Wehmas LC, et al. Microbiota alter metabolism and mediate
735 neurodevelopmental toxicity of 17beta-estradiol. Sci Rep 2019;9:7064.
736 13. Kim E, Paik D, Ramirez RN, et al. Maternal gut bacteria drive intestinal inflammation in offspring
737 with neurodevelopmental disorders by altering the chromatin landscape of CD4(+) T cells.
738 Immunity 2022;55:145-158 e7.
739 14. Cho HM, Gonzalez-Ortiz G, Melo-Duran D, et al. Stimbiotic supplementation improved
740 performance and reduced inflammatory response via stimulating fiber fermenting microbiome
741 in weaner pigs housed in a poor sanitary environment and fed an antibiotic-free low zinc oxide
742 diet. PLoS One 2020;15:e0240264.
743 15. Everard A, Belzer C, Geurts L, et al. Cross-talk between Akkermansia muciniphila and intestinal
744 epithelium controls diet-induced obesity. Proc Natl Acad Sci U S A 2013;110:9066-71.
745 16. Lee H, Lee Y, Kim J, et al. Modulation of the gut microbiota by metformin improves metabolic
746 profiles in aged obese mice. Gut Microbes 2018;9:155-165.
747 17. Rodrigues RR, Greer RL, Dong X, et al. Antibiotic-Induced Alterations in Gut Microbiota Are
748 Associated with Changes in Glucose Metabolism in Healthy Mice. Front Microbiol 2017;8:2306.
749 18. Desbonnet L, Clarke G, Shanahan F, et al. Microbiota is essential for social development in the
750 mouse. Mol Psychiatry 2014;19:146-8.
751 19. Diaz Heijtz R, Wang S, Anuar F, et al. Normal gut microbiota modulates brain development and
752 behavior. Proc Natl Acad Sci U S A 2011;108:3047-52.
753 20. Rabot S, Membrez M, Bruneau A, et al. Germ-free C57BL/6J mice are resistant to high-fat-diet-
754 induced insulin resistance and have altered cholesterol metabolism. FASEB J 2010;24:4948-59.
755 21. Collins SM, Kassam Z, Bercik P. The adoptive transfer of behavioral phenotype via the intestinal
756 microbiota: experimental evidence and clinical implications. Curr Opin Microbiol 2013;16:240-5.
757 22. De Palma G, Lynch MD, Lu J, et al. Transplantation of fecal microbiota from patients with irritable
758 bowel syndrome alters gut function and behavior in recipient mice. Sci Transl Med 2017;9.
759 23. Turnbaugh PJ, Ley RE, Mahowald MA, et al. An obesity-associated gut microbiome with
760 increased capacity for energy harvest. Nature 2006;444:1027-31.
761 24. Pessa-Morikawa T, Husso A, Karkkainen O, et al. Maternal microbiota-derived metabolic profile
762 in fetal murine intestine, brain and placenta. BMC Microbiol 2022;22:46.
763 25. Deng X, Guarita DR, Pedroso MR, et al. PYY inhibits CCK-stimulated pancreatic secretion through
764 the area postrema in unanesthetized rats. Am J Physiol Regul Integr Comp Physiol
765 2001;281:R645-53.
766 26. Cabral A, Cornejo MP, Fernandez G, et al. Circulating Ghrelin Acts on GABA Neurons of the Area
767 Postrema and Mediates Gastric Emptying in Male Mice. Endocrinology 2017;158:1436-1449.

768 27. Yamamoto H, Kishi T, Lee CE, et al. Glucagon-like peptide-1-responsive catecholamine neurons in
769 the area postrema link peripheral glucagon-like peptide-1 with central autonomic control sites. J
770 Neurosci 2003;23:2939-46.
771 28. Arslanova A, Tarasova A, Alexandrova A, et al. Protective Effects of Probiotics on Cognitive and
772 Motor Functions, Anxiety Level, Visceral Sensitivity, Oxidative Stress and Microbiota in Mice with
773 Antibiotic-Induced Dysbiosis. Life (Basel) 2021;11.
774 29. O'Connor R, Moloney GM, Fulling C, et al. Maternal antibiotic administration during a critical
775 developmental window has enduring neurobehavioural effects in offspring mice. Behav Brain
776 Res 2021;404:113156.
777 30. Sun Y, Zhu H, Cheng R, et al. Outer membrane protein Amuc_1100 of Akkermansia muciniphila
778 alleviates antibiotic-induced anxiety and depression-like behavior in mice. Physiol Behav
779 2023;258:114023.
780 31. Bruce-Keller AJ, Fernandez-Kim SO, Townsend RL, et al. Maternal obese-type gut microbiota
781 differentially impact cognition, anxiety and compulsive behavior in male and female offspring in
782 mice. PLoS One 2017;12:e0175577.
783 32. Cheatham CN, Gustafson KL, McAdams ZL, et al. Standardized Complex Gut Microbiomes
784 Influence Fetal Growth, Food Intake, and Adult Body Weight in Outbred Mice. Microorganisms
785 2023;11.
786 33. Ericsson AC, Davis JW, Spollen W, et al. Effects of vendor and genetic background on the
787 composition of the fecal microbiota of inbred mice. PLoS One 2015;10:e0116704.
788 34. Ericsson AC, Hart ML, Kwan J, et al. Supplier-origin mouse microbiomes significantly influence
789 locomotor and anxiety-related behavior, body morphology, and metabolism. Commun Biol
790 2021;4:716.
791 35. Song Z, Cai Y, Lao X, et al. Taxonomic profiling and populational patterns of bacterial bile salt
792 hydrolase (BSH) genes based on worldwide human gut microbiome. Microbiome 2019;7:9.
793 36. Abdulrab S, Al-Maweri S, Halboub E. Ursodeoxycholic acid as a candidate therapeutic to alleviate
794 and/or prevent COVID-19-associated cytokine storm. Med Hypotheses 2020;143:109897.
795 37. Adhikari A, Topiwala MA, Gordon JA. Synchronized activity between the ventral hippocampus
796 and the medial prefrontal cortex during anxiety. Neuron 2010;65:257-69.
797 38. Baksh RA, Ritchie CW, Terrera GM, et al. The association between anxiety disorders and
798 hippocampal volume in older adults. Psychol Aging 2021;36:288-297.
799 39. Jimenez JC, Su K, Goldberg AR, et al. Anxiety Cells in a Hippocampal-Hypothalamic Circuit.
800 Neuron 2018;97:670-683 e6.
801 40. Mineur YS, Obayemi A, Wigestrand MB, et al. Cholinergic signaling in the hippocampus regulates
802 social stress resilience and anxiety- and depression-like behavior. Proc Natl Acad Sci U S A
803 2013;110:3573-8.
804 41. Revest JM, Dupret D, Koehl M, et al. Adult hippocampal neurogenesis is involved in anxiety-
805 related behaviors. Mol Psychiatry 2009;14:959-67.
806 42. Satpute AB, Mumford JA, Naliboff BD, Poldrack RA. Human anterior and posterior hippocampus
807 respond distinctly to state and trait anxiety. Emotion 2012;12:58-68.
808 43. Wolfe AE, Moskowitz JE, Franklin CL, et al. Interactions of Segmented Filamentous Bacteria
809 (Candidatus Savagella) and bacterial drivers in colitis-associated colorectal cancer development.
810 PLoS One 2020;15:e0236595.
811 44. Cantor JR, Abu-Remaileh M, Kanarek N, et al. Physiologic Medium Rewires Cellular Metabolism
812 and Reveals Uric Acid as an Endogenous Inhibitor of UMP Synthase. Cell 2017;169:258-272.e17.
813 45. Li B, Tang J, Yang Q, et al. NOREVA: normalization and evaluation of MS-based metabolomics
814 data. Nucleic Acids Res 2017;45:W162-w170.

815 46. Walters WA, Caporaso JG, Lauber CL, et al. PrimerProspector: de novo design and taxonomic
816 analysis of barcoded polymerase chain reaction primers. Bioinformatics 2011;27:1159-61.
817 47. Caporaso JG, Lauber CL, Walters WA, et al. Global patterns of 16S rRNA diversity at a depth of
818 millions of sequences per sample. Proc Natl Acad Sci U S A 2011;108 Suppl 1:4516-22.
819 48. Loy A, Maixner F, Wagner M, Horn M. probeBase--an online resource for rRNA-targeted
820 oligonucleotide probes: new features 2007. Nucleic Acids Res 2007;35:D800-4.
821 49. Martin M. Cutadapt removes adapter sequences from high-throughput sequencing reads.
822 EMBnet.journal 2011;17:10-12.
823 50. Bolyen E, Rideout JR, Dillon MR, et al. Reproducible, interactive, scalable and extensible
824 microbiome data science using QIIME 2. Nat Biotechnol 2019;37:852-857.
825 51. Callahan BJ, McMurdie PJ, Rosen MJ, et al. DADA2: High-resolution sample inference from
826 Illumina amplicon data. Nat Methods 2016;13:581-3.
827 52. Pruesse E, Quast C, Knittel K, et al. SILVA: a comprehensive online resource for quality checked
828 and aligned ribosomal RNA sequence data compatible with ARB. Nucleic Acids Res
829 2007;35:7188-96.
830 53. Zachary L McAdams SBB, Kevin L Gustafson, Nathan Bivens, Craig L Franklin, Paul Wilmes, Aaron
831 C Ericsson. Multi-omics analysis of mouse fecal microbiome reveals supplier-dependent
832 functional differences and novel metagenome-assembled genomes. bioRxiv 2022.
833 54. Khodakivskyi PV, Lauber CL, Yevtodiyenko A, et al. Noninvasive imaging and quantification of bile
834 salt hydrolase activity: From bacteria to humans. Sci Adv 2021;7.
835 55. Vorobyeva AG, Stanton M, Godinat A, et al. Development of a Bioluminescent Nitroreductase
836 Probe for Preclinical Imaging. PLoS One 2015;10:e0131037.
837 56. Wolock SL, Lopez R, Klein AM. Scrublet: Computational Identification of Cell Doublets in Single-
838 Cell Transcriptomic Data. Cell Syst 2019;8:281-291 e9.
839 57. Stuart T, Butler A, Hoffman P, et al. Comprehensive Integration of Single-Cell Data. Cell
840 2019;177:1888-1902 e21.
841 58. Team RDC. R: A Language and Environment for Statistical Computing. 2010.
842 59. Jin S, Guerrero-Juarez CF, Zhang L, et al. Inference and analysis of cell-cell communication using
843 CellChat. Nat Commun 2021;12:1088.
844 60. Suoqin J, Maksim VP, Qing N. CellChat for systematic analysis of cell-cell communication from
845 single-cell and spatially resolved transcriptomics. bioRxiv 2023:2023.11.05.565674.
846 61. Zhou W, Hinoue T, Barnes B, et al. DNA methylation dynamics and dysregulation delineated by
847 high-throughput profiling in the mouse. Cell Genom 2022;2.
848 62. Xu Z, Niu L, Li L, Taylor JA. ENmix: a novel background correction method for Illumina
849 HumanMethylation450 BeadChip. Nucleic Acids Res 2016;44:e20.
850 63. Aryee MJ, Jaffe AE, Corrada-Bravo H, et al. Minfi: a flexible and comprehensive Bioconductor
851 package for the analysis of Infinium DNA methylation microarrays. Bioinformatics 2014;30:1363-
852 9.
853 64. Xu Z, Langie SA, De Boever P, et al. RELIC: a novel dye-bias correction method for Illumina
854 Methylation BeadChip. BMC Genomics 2017;18:4.

855

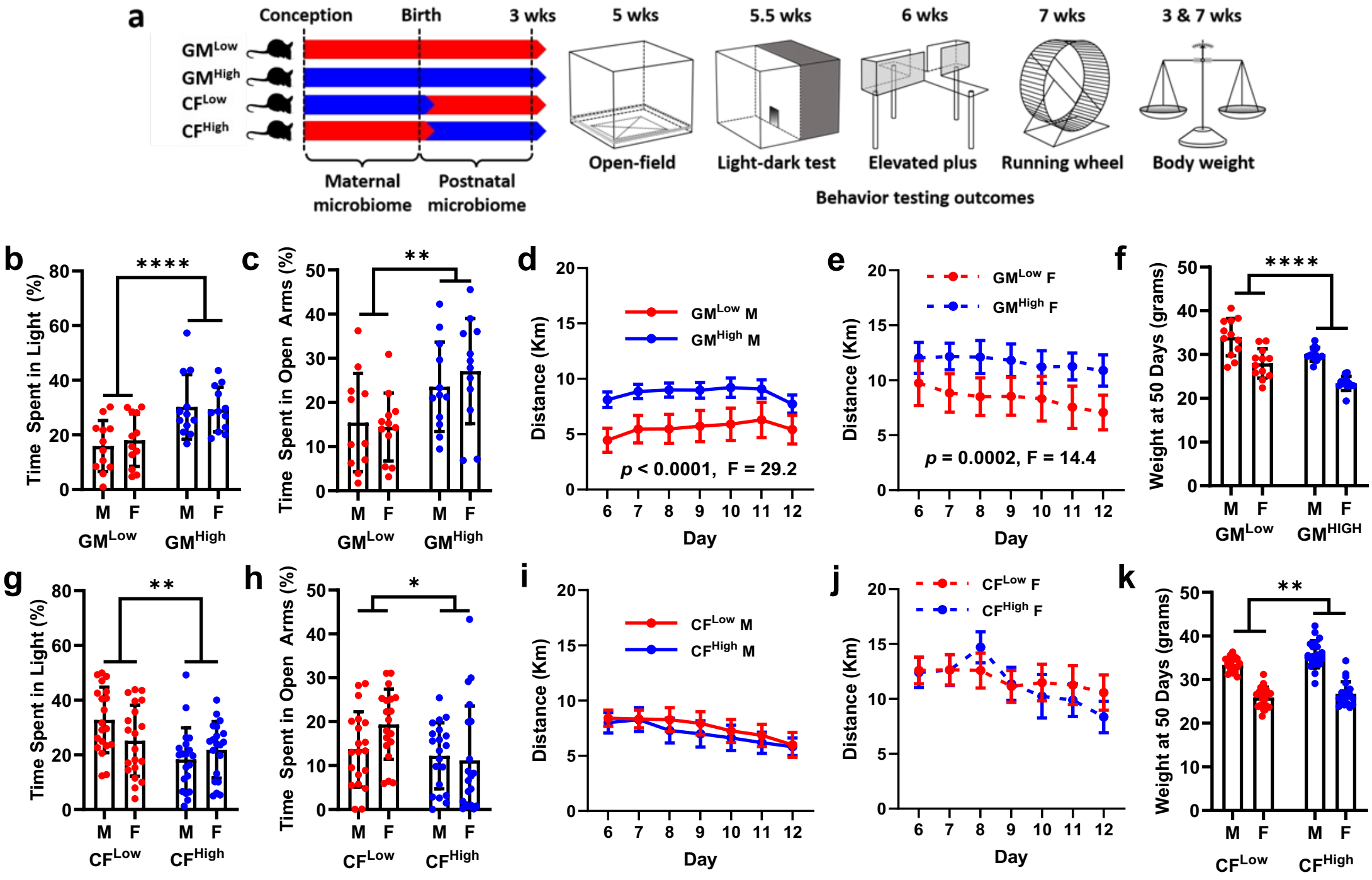
a
Conception
Birth
3 wks
5 wks
5.5 wks
6 wks
7 wks
3 & 7 wks
GM^Low
GM^High
CF^Low
CF^High
Maternal microbiome
Postnatal microbiome
Open-field
Light-dark test
Elevated plus
Running wheel
Body weight
Behavior testing outcomes
b
Time Spent in Light (%)
****
M F M F
GM^Low GM^High
c
Time Spent in Open Arms (%)
**
M F M F
GM^Low GM^High
d
Distance (Km)
GM^Low M
GM^High M
p < 0.0001, F = 29.2
Day
e
Distance (Km)
GM^Low F
GM^High F
p = 0.0002, F = 14.4
Day
f
Weight at 50 Days (grams)
****
M F M F
GM^Low GM^HIGH
g
Time Spent in Light (%)
**
M F M F
CF^Low CF^High
h
Time Spent in Open Arms (%)
*
M F M F
CF^Low CF^High
i
Distance (Km)
CF^Low M
CF^High M
Day
j
Distance (Km)
CF^Low F
CF^High F
Day
k
Weight at 50 Days (grams)
**
M F M F
CF^Low CF^High

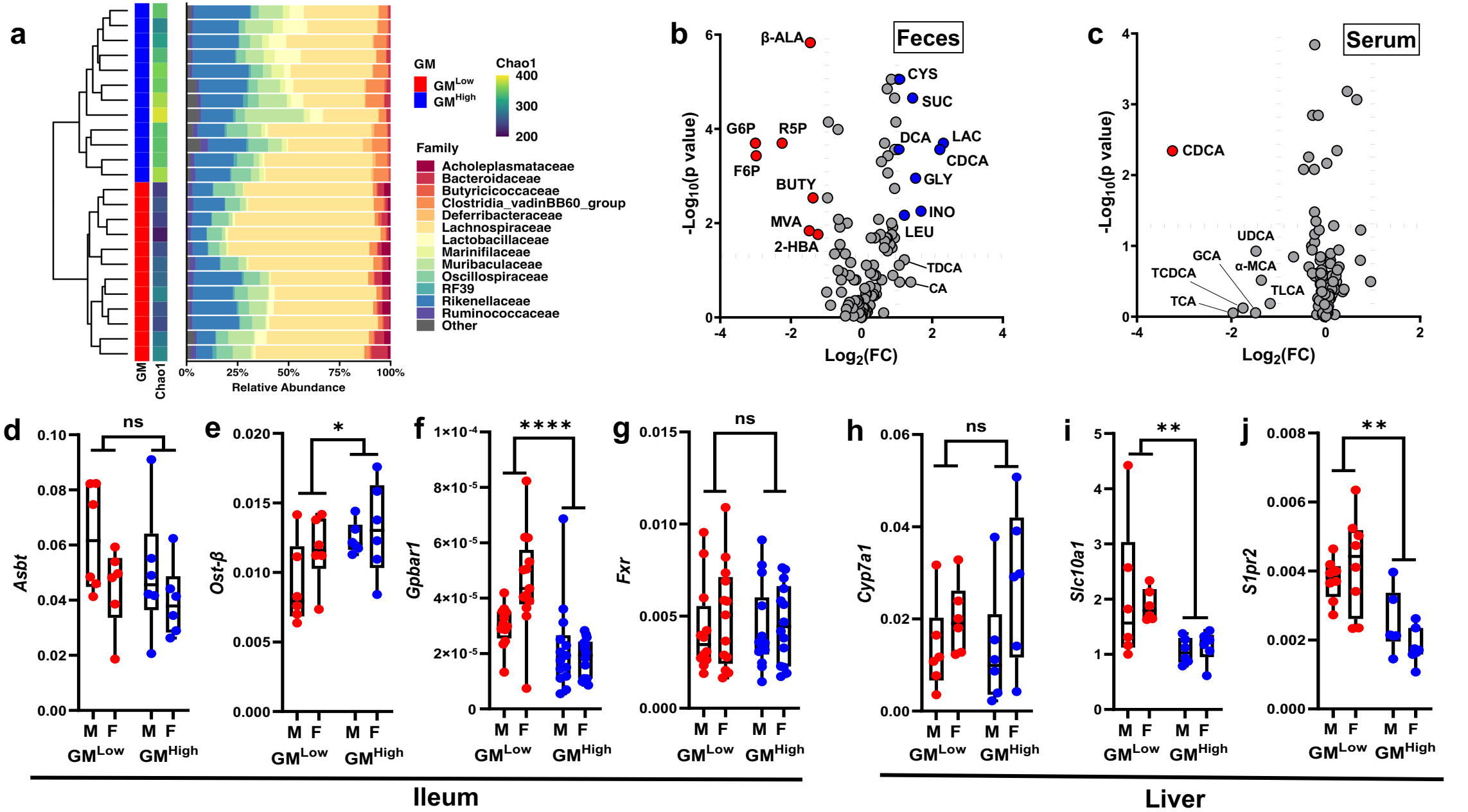
a
GM
GM^Low
GM^High
Chao1
400
300
200
Family
Acholeplasmataceae
Bacteroidaceae
Butyricicoccaceae
Clostridia_vadinBB60_group
Deferribacteraceae
Lachnospiraceae
Lactobacillaceae
Marinifilaceae
Muribaculaceae
Oscillospiraceae
RF39
Rikenellaceae
Ruminococcaceae
Other
0%
25%
50%
75%
100%
Relative Abundance
b
Feces
β-ALA
CYS
SUC
G6P
R5P
F6P
DCA
LAC
CDCA
BUTY
GLY
MVA
2-HBA
INO
LEU
TDCA
CA
-Log10(p value)
Log2(FC)
c
Serum
CDCA
UDCA
GCA
α-MCA
TCDCA
TLCA
TCA
-Log10(p value)
Log2(FC)
d
ns
Asbt
e
*
Ost-β
f
****
Gpbar1
g
ns
Fxr
h
ns
Cyp7a1
i
**
Slc10a1
j
**
S1pr2
M F M F
GM^Low GM^High
Ileum
Liver

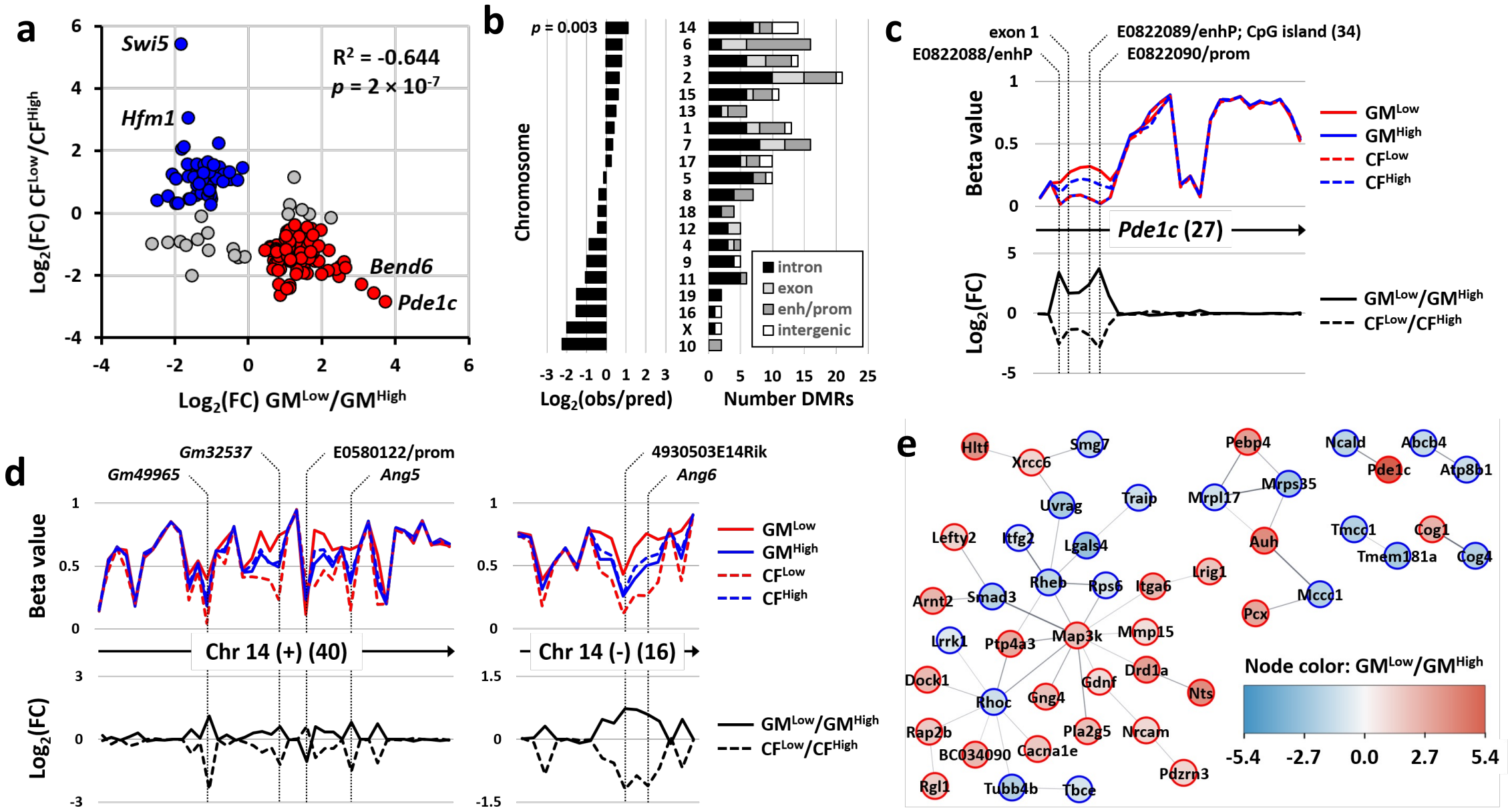
a
Swi5
Hfm1
Bend6
Pde1c
R² = -0.644
p = 2 × 10⁻⁷
Log2(FC) CFLow/CFHigh
Log2(FC) GMLow/GMHigh
b
p = 0.003
Chromosome
Log2(obs/pred)
Number DMRs
intron
exon
enh/prom
intergenic
c
exon 1
E0822088/enhP
E0822089/enhP; CpG island (34)
E0822090/prom
Beta value
Pde1c (27)
Log2(FC)
GMLow
GMHigh
CFLow
CFHigh
GMLow/GMHigh
CFLow/CFHigh
d
Gm32537
Gm49965
E0580122/prom
Ang5
Chr 14 (+) (40)
4930503E14Rik
Ang6
Chr 14 (-) (16)
Beta value
Log2(FC)
GMLow
GMHigh
CFLow
CFHigh
GMLow/GMHigh
CFLow/CFHigh
e
Hltf
Smg7
Xrcc6
Uvrag
Traip
Lefty2
Itfg2
Lgals4
Rheb
Rps6
Itga6
Arnt2
Smad3
Map3k
Mmp15
Lrrk1
Ptp4a3
Drd1a
Dock1
Gdnf
Rhoc
Gng4
Nts
Rap2b
Pla2g5
Nrcam
BC034090
Cacna1e
Pdzrn3
Rgl1
Tubb4b
Tbce
Pebp4
Ncald
Abcb4
Pde1c
Atp8b1
Mrps35
Mrpl17
Auh
Tmcc1
Cog1
Tmem181a
Cog4
Lrig1
Mccc1
Pcx
Node color: GMLow/GMHigh
-5.4
-2.7
0.0
2.7
5.4

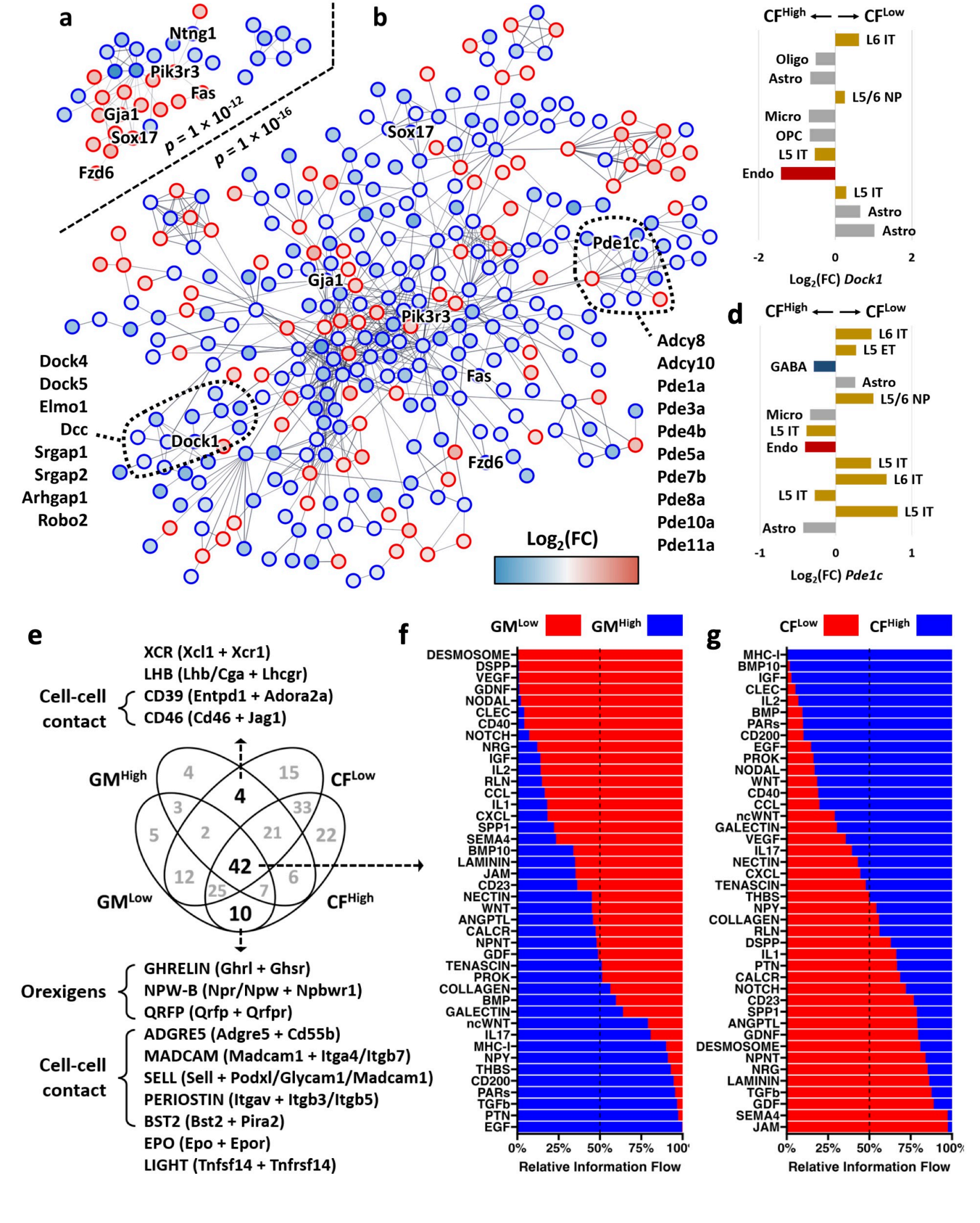
a
Ntng1
Pik3r3
Fas
Gja1
Sox17
Fzd6
p = 1 x 10-12
p = 1 x 10-16
b
Sox17
Gja1
Pik3r3
Fas
Fzd6
Pde1c
Dock1
Dock4
Dock5
Elmo1
Dcc
Srgap1
Srgap2
Arhgap1
Robo2
Adcy8
Adcy10
Pde1a
Pde3a
Pde4b
Pde5a
Pde7b
Pde8a
Pde10a
Pde11a
Log2(FC)
CFHigh ← → CFLow
L6 IT
Oligo
Astro
L5/6 NP
Micro
OPC
L5 IT
Endo
L5 IT
Astro
Astro
-2
0
2
Log2(FC) Dock1
d
CFHigh ← → CFLow
L6 IT
L5 ET
GABA
Astro
L5/6 NP
Micro
L5 IT
Endo
L5 IT
L6 IT
L5 IT
L5 IT
Astro
-1
0
1
Log2(FC) Pde1c
e
Cell-cell contact
XCR (Xcl1 + Xcr1)
LHB (Lhb/Cga + Lhcgr)
CD39 (Entpd1 + Adora2a)
CD46 (Cd46 + Jag1)
GMHigh
CFLow
GMLow
CFHigh
4
15
3
4
33
5
2
21
22
42
12
6
25
7
10
Orexigens
GHRELIN (Ghrl + Ghsr)
NPW-B (Npr/Npw + Npbwr1)
QRFP (Qrfp + Qrfpr)
Cell-cell contact
ADGRE5 (Adgre5 + Cd55b)
MADCAM (Madcam1 + Itga4/Itgb7)
SELL (Sell + Podxl/Glycam1/Madcam1)
PERIOSTIN (Itgav + Itgb3/Itgb5)
BST2 (Bst2 + Pira2)
EPO (Epo + Epor)
LIGHT (Tnfsf14 + Tnfrsf14)
f
GMLow
GMHigh
DESMOSOME
DSPP
VEGF
GDNF
NODAL
CLEC
CD40
NOTCH
NRG
IGF
IL2
RLN
CCL
IL1
CXCL
SPP1
SEMA4
BMP10
LAMININ
JAM
CD23
NECTIN
WNT
ANGPTL
CALCR
NPNT
GDF
TENASCIN
PROK
COLLAGEN
BMP
GALECTIN
ncWNT
IL17
MHC-I
NPY
THBS
CD200
PARs
TGFb
PTN
EGF
0%
25%
50%
75%
100%
Relative Information Flow
g
CFLow
CFHigh
MHC-I
BMP10
IGF
CLEC
IL2
BMP
PARs
CD200
EGF
PROK
NODAL
WNT
CD40
CCL
ncWNT
GALECTIN
VEGF
IL17
NECTIN
CXCL
TENASCIN
THBS
NPY
COLLAGEN
RLN
DSPP
IL1
PTN
CALCR
NOTCH
CD23
SPP1
ANGPTL
GDNF
DESMOSOME
NPNT
NRG
LAMININ
TGFb
GDF
SEMA4
JAM
0%
25%
50%
75%
100%
Relative Information Flow

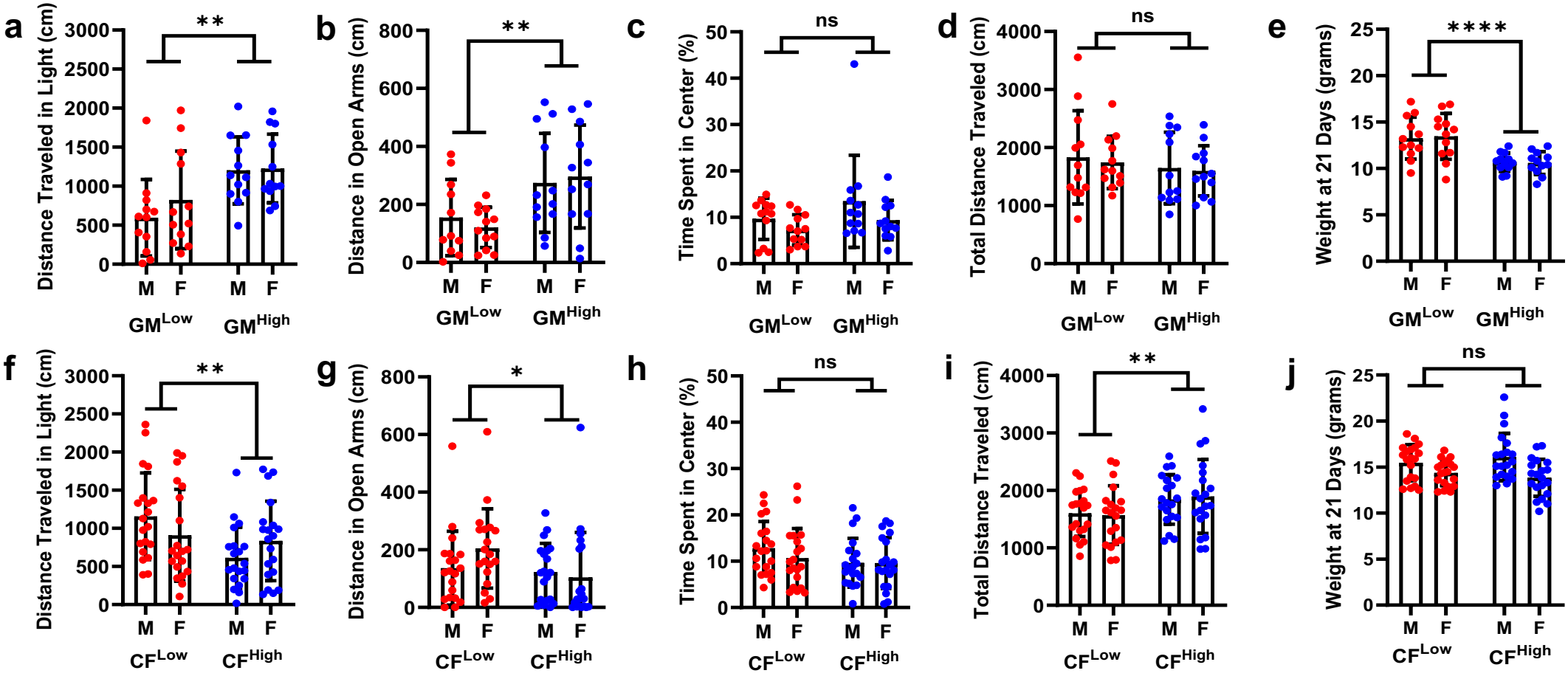
a
Distance Traveled in Light (cm)
3000
2500
2000
1500
1000
500
0
**
M F M F
GMLow GMHigh
b
Distance in Open Arms (cm)
800
600
400
200
0
**
M F M F
GMLow GMHigh
c
Time Spent in Center (%)
50
40
30
20
10
0
ns
M F M F
GMLow GMHigh
d
Total Distance Traveled (cm)
4000
3000
2000
1000
0
ns
M F M F
GMLow GMHigh
e
Weight at 21 Days (grams)
25
20
15
10
5
0
****
M F M F
GMLow GMHigh
f
Distance Traveled in Light (cm)
3000
2500
2000
1500
1000
500
0
**
M F M F
CFLow CFHigh
g
Distance in Open Arms (cm)
800
600
400
200
0
*
M F M F
CFLow CFHigh
h
Time Spent in Center (%)
50
40
30
20
10
0
ns
M F M F
CFLow CFHigh
i
Total Distance Traveled (cm)
4000
3000
2000
1000
0
**
M F M F
CFLow CFHigh
j
Weight at 21 Days (grams)
25
20
15
10
5
0
ns
M F M F
CFLow CFHigh

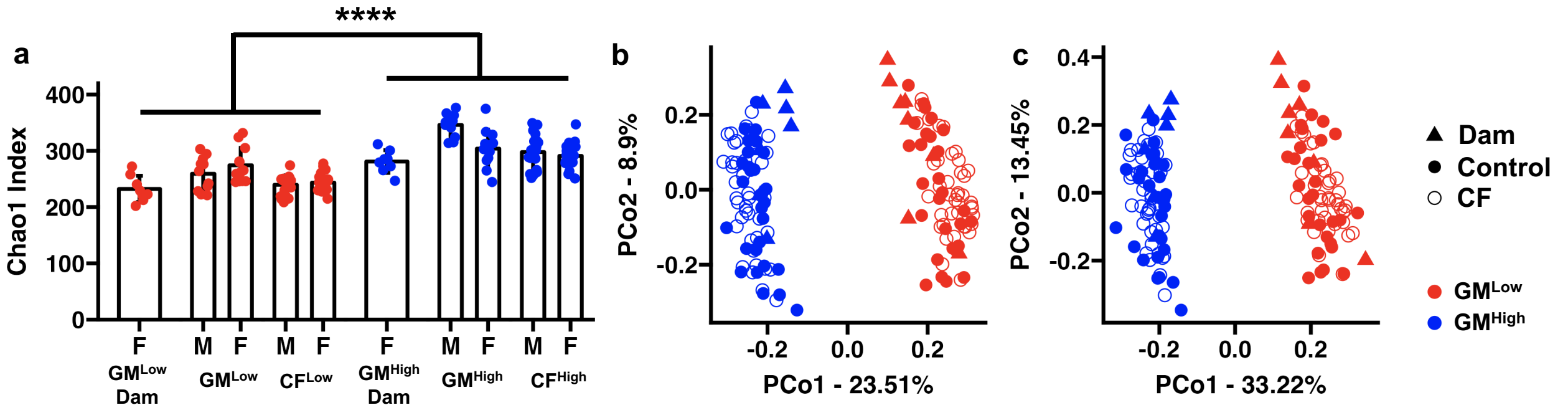
a
****
Chao1 Index
400
300
200
100
0
F
M
F
M
F
F
M
F
M
F
GMLow Dam
GMLow
CFLow
GMHigh Dam
GMHigh
CFHigh
b
PCo2 - 8.9%
0.2
0.0
-0.2
-0.2
0.0
0.2
PCo1 - 23.51%
c
PCo2 - 13.45%
0.4
0.2
0.0
-0.2
-0.2
0.0
0.2
PCo1 - 33.22%
Dam
Control
CF
GMLow
GMHigh

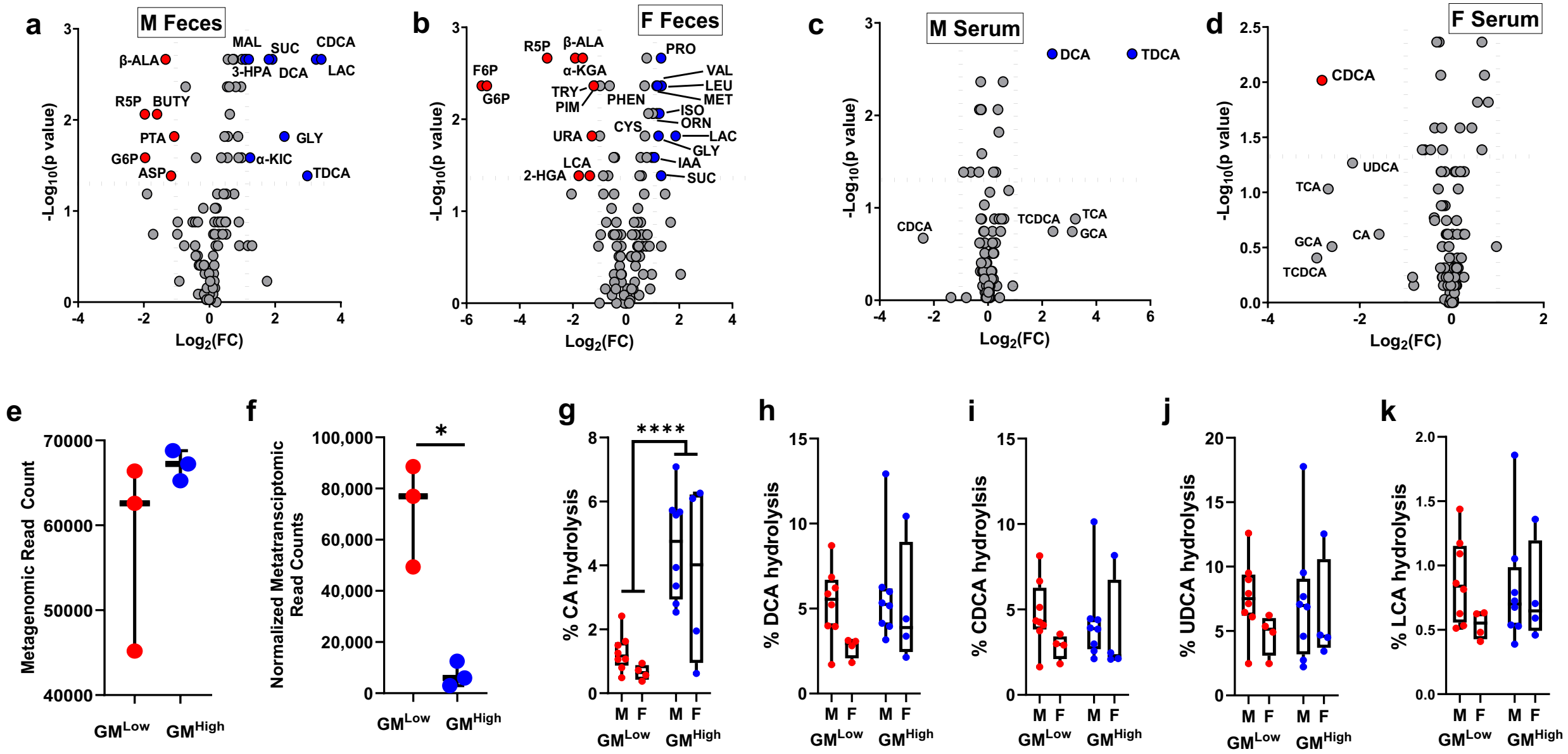
a
M Feces
β-ALA
MAL
SUC
CDCA
3-HPA
DCA
LAC
R5P
BUTY
PTA
GLY
G6P
α-KIC
ASP
TDCA
-Log10(p value)
Log2(FC)
b
F Feces
R5P
β-ALA
PRO
F6P
α-KGA
VAL
G6P
TRY
LEU
PIM
PHEN
MET
ISO
CYS
ORN
URA
LAC
GLY
LCA
IAA
2-HGA
SUC
c
M Serum
DCA
TDCA
CDCA
TCDCA
TCA
GCA
d
F Serum
CDCA
UDCA
TCA
CA
GCA
TCDCA
e
Metagenomic Read Count
GMLow
GMHigh
f
Normalized Metatranscriptomic Read Counts
*
g
****
% CA hydrolysis
h
% DCA hydrolysis
i
% CDCA hydroylsis
j
% UDCA hydrolysis
k
% LCA hydrolysis
M F M F
GMLow GMHigh

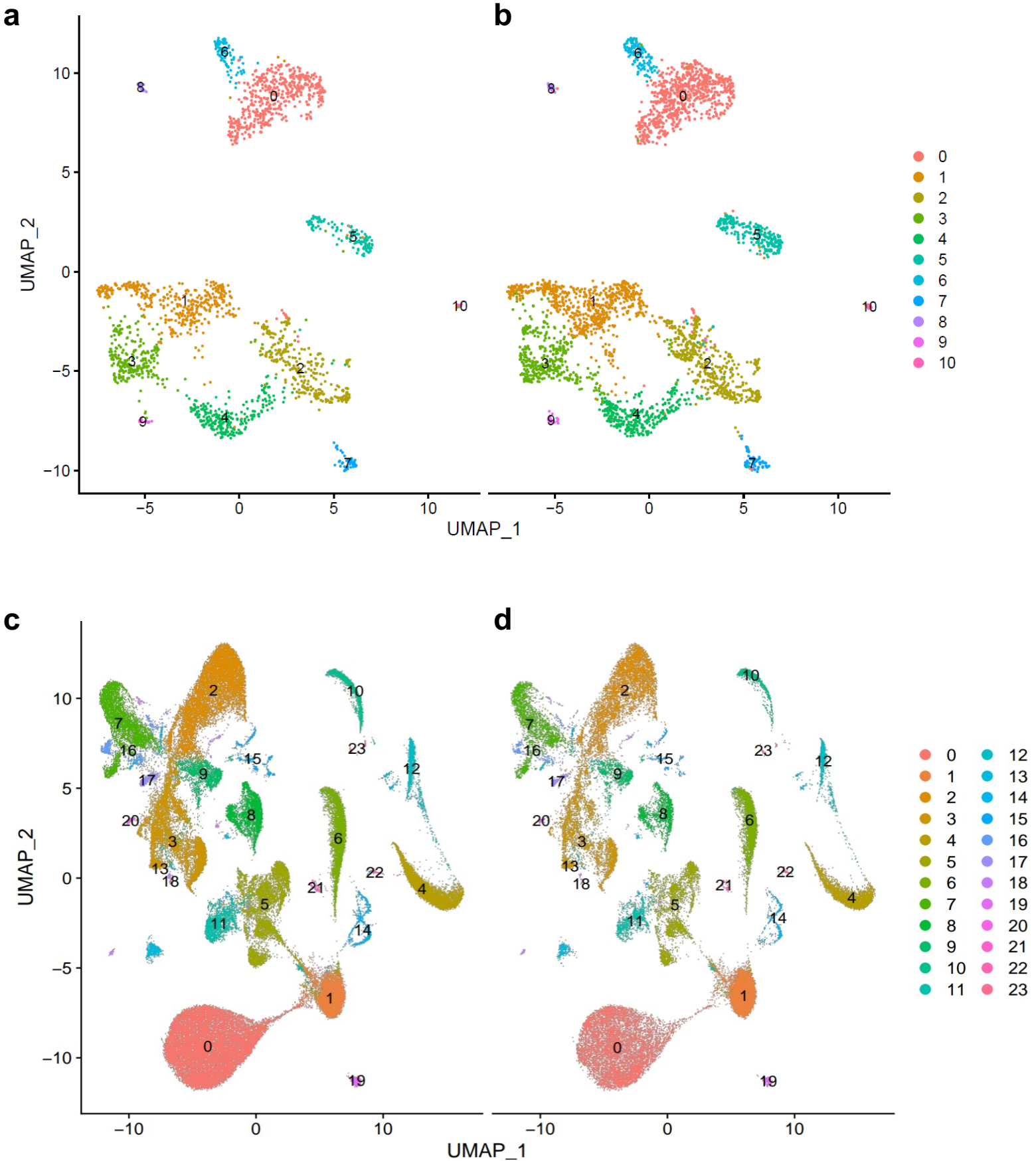
a
b
c
d
UMAP_1
UMAP_2
0
1
2
3
4
5
6
7
8
9
10
11
12
13
14
15
16
17
18
19
20
21
22
23

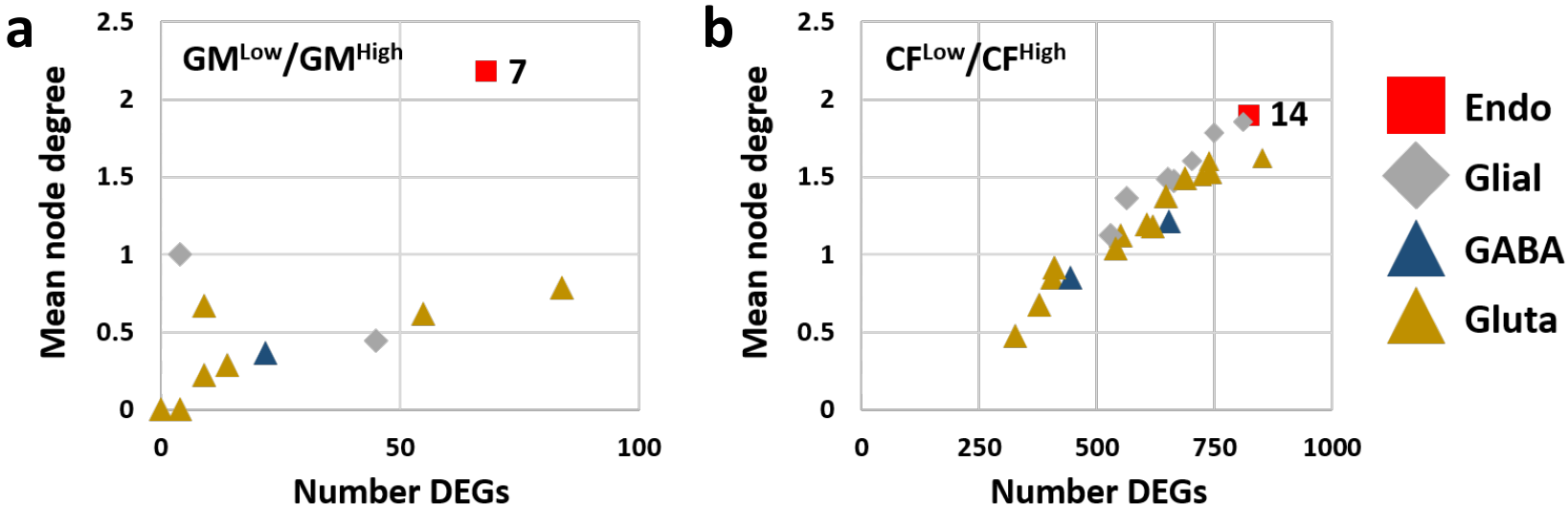
a
GMLow/GMHigh
7
Mean node degree
Number DEGs
2.5
2
1.5
1
0.5
0
0
50
100
b
CFLow/CFHigh
14
Mean node degree
Number DEGs
2.5
2
1.5
1
0.5
0
0
250
500
750
1000
Endo
Glial
GABA
Gluta

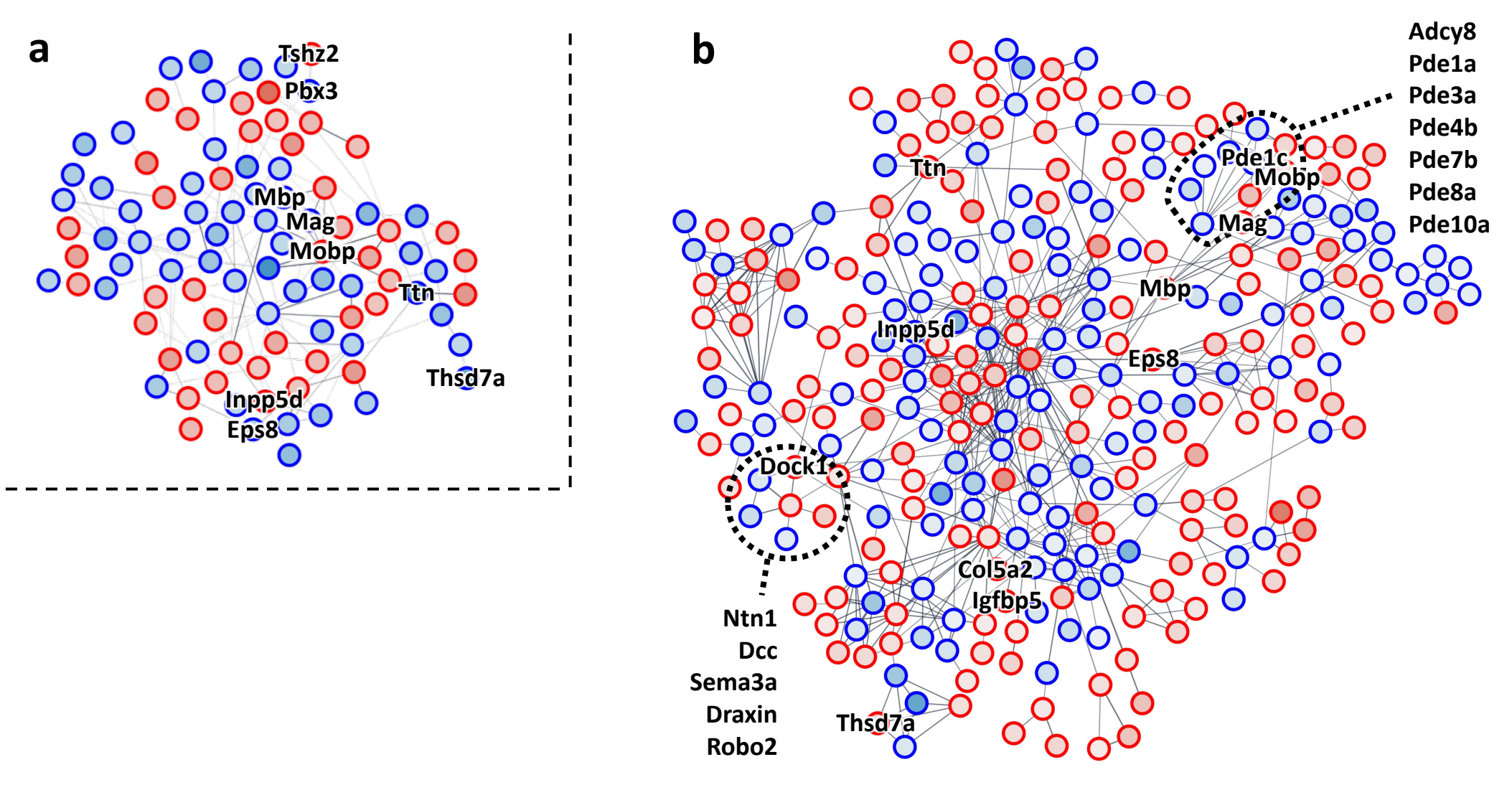
a
Tshz2
Pbx3
Mbp
Mag
Mobp
Ttn
Thsd7a
Inpp5d
Eps8
b
Adcy8
Pde1a
Pde3a
Pde4b
Pde7b
Pde8a
Pde10a
Pde1c
Mobp
Mag
Ttn
Mbp
Inpp5d
Eps8
Dock1
Col5a2
Igfbp5
Ntn1
Dcc
Sema3a
Draxin
Robo2
Thsd7a

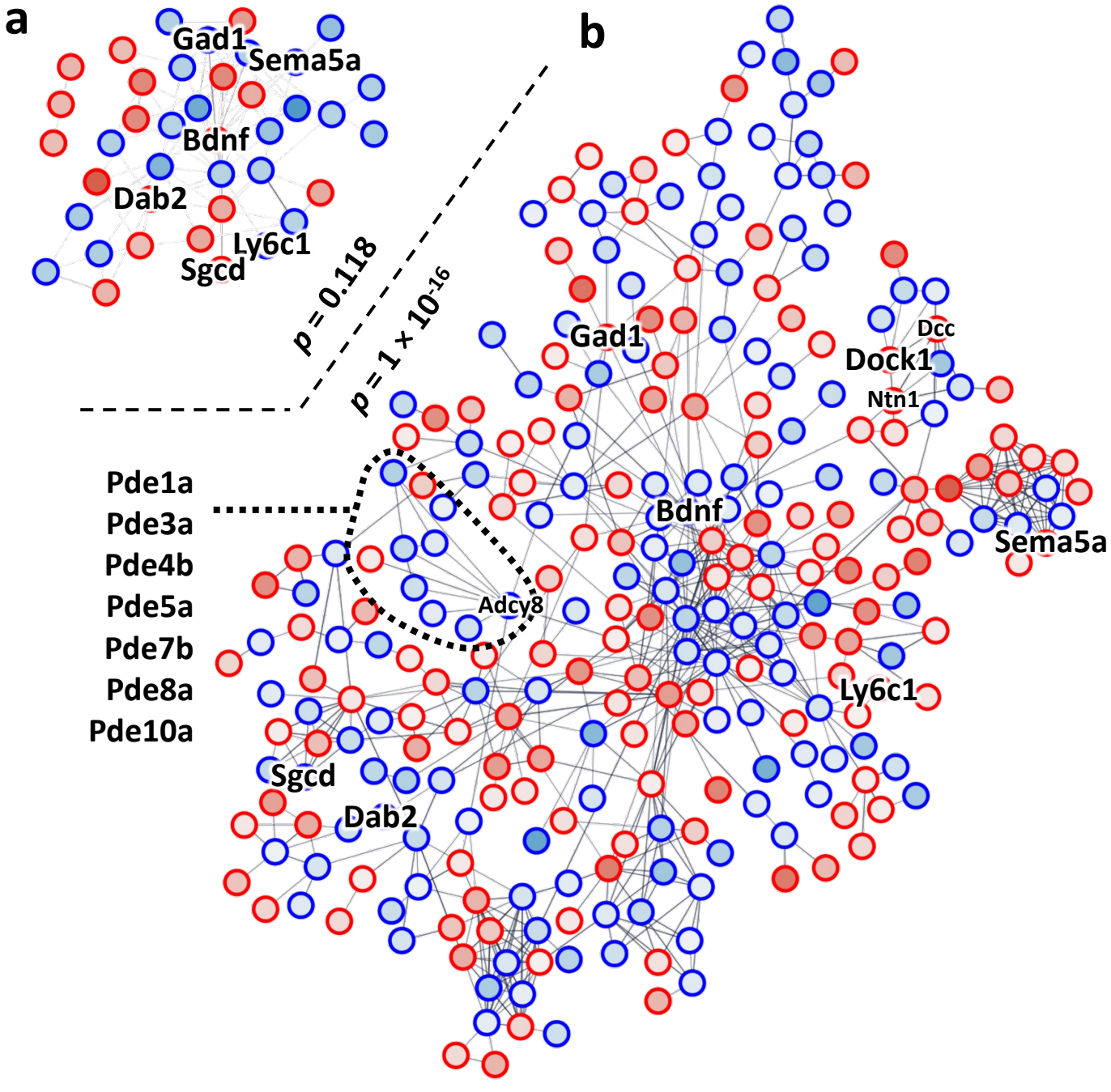
a
Gad1
Sema5a
Bdnf
Dab2
Ly6c1
Sgcd
p = 0.118
p = 1 × 10-16
b
Gad1
Dcc
Dock1
Ntn1
Pde1a
Pde3a
Pde4b
Pde5a
Pde7b
Pde8a
Pde10a
Bdnf
Sema5a
Adcy8
Ly6c1
Sgcd
Dab2